Genetic and Molecular Analysis of dec-11 in C. elegans' Intestinal Pacemaker Activity

Adele Joan Gordon
Marquette University

GENETIC AND MOLECULAR ANALYSIS OF *dec-11* IN *C. elegans'* INTESTINAL PACEMAKER ACTIVITY

By
Adele J Gordon, B.S.

A Thesis submitted to the Faculty of the Graduate School,
Marquette University,
in Partial Fulfillment of the Requirements for
the Degree of Master of Science

Milwaukee, Wisconsin

May 2015

ABSTRACT
GENETIC AND MOLECULAR ANALYSIS OF *dec-11* IN *C. elegans'* INTESTINAL PACEMAKER ACTIVITY

Adele J Gordon, B.S.

Marquette University, 2015

Rhythmic behaviors are ubiquitous phenomena in plant and animal phyla. Ultradian rhythmic behaviors occur with a period of less than 24 hours and include such rhythmic behaviors as the beating of the heart and peristalsis in the gut. The nematode *C. elegans* exhibits three well-characterized ultradian rhythmic behaviors: ovulation, pharyngeal pumping, and the defecation motor program (DMP). The DMP occurs every ~45 seconds in wild-type worms and comprises three distinct muscle contractions: a posterior body contraction (pBoc), an anterior body contraction (aBoc), and an enteric muscle contraction (Emc), which is coupled to expulsion (Exp). The rhythmicity of the DMP is Ca^{2+}-dependent, meaning fluctuations in intracellular Ca^{2+} levels in the pacemaker cell regulate the behavior.

A forward genetic screen was performed to identify genes necessary for proper pacemaker function (Iwasaki et al., 1995). One of the mutants isolated, *dec-11*, lacks pacemaker activity and displays long and irregular defecation cycles. However, the gene mutated in *dec-11* worms has not been identified. In order to determine the function of the *dec-11* gene in the control of pacemaker activity for the DMP, genetic analysis and video microscopy were utilized. First, genetic analysis was performed to test whether *dec-11* acts upstream of IP_3 mediated Ca^{2+} release using mutations in *ipp-5* and *lfe-2*, which encode an IP_3 phosphatase and an IP_3 kinase respectively. *dec-11;ipp-5* and *dec-11;lfe-2* double mutants both showed partial suppression of the irregular defecation cycle phenotype characteristic of *dec-11* single mutants. Additionally, when *dec-11* worms were grown on high Mg^{2+} plates, the irregular defecation cycles were suppressed, suggesting a role for *dec-11* in the regulation of the DMP. Parallel work using SNP interval mapping and whole-genome sequencing has allowed us to identify a molecular interval in which *dec*-11 is located and to generate a list of candidate genes. Additionally, RNAi analysis of candidate genes will allow us to determine the molecular identity of *dec-11*. Taken together these data are consistent with a model that places the function of *dec-11* in the regulation of the initiating event of the DMP.

ACKNOWLEDGEMENTS

Adele J Gordon, B.S.

I would first like to thank the members of my committee, Drs Allison Abbott, Edward Blumenthal, and Lisa Petrella. I have had the good fortune and pleasure of working with three extremely intelligent, clever, and supportive faculty members. Thank you for your support, your insight, and all your suggestions. I would particularly like to thank Dr. Abbott, my advisor, for her invaluable support over these last three years as a researcher and as a stand-in mother while I have been away from home. A thousand times, thank you.

I would also like to thank Michael Lim, Jamie Collins, and Katalin Kenney, three undergraduates, who helped with generating and collecting data. Michael Lim assisted with data collection for the SNP interval mapping. Jamie Collins and Katalin Kenney helped with RNAi defecation scoring of *dec-11* candidate genes.

I would especially like to thank my parents, Percy and Jane Gordon for their constant support and belief that I can do anything I set my mind to. Your belief in me, and selfless sacrifices for the past 26 years have allowed me to pursue my passions and interests. I have tried to make you both proud and I hope that I have succeeded. I love you both and I am so thankful to call you Muttie and Poppie.

Last but not least, it gives me great pleasure to acknowledge and thank my significant other Charles Janicki. Charlie, without your unending support and comfort, graduate school would have been all the harder. Without you, this document would remain unfinished, and I would have starved to death. I will never really be able to adequately thank you for all the things you have done for me over the past three years, but I hope that in this small way you will know how much it all meant to me. You are my best friend and I love you endlessly.

TABLE OF CONTENTS

I. INTRODUCTION

Examples of rhythmic behaviors are found throughout plant and animal phyla. Rhythmic behaviors can be classified into three types: Infradian, Circadian, and Ultradian. Infradian rhythms have a period greater than 24 hours; examples of infradian rhythms include annual whale or fowl migrations. Circadian rhythms, which have a period of 24 hours, include behaviors such as sleep cycles in mammals, photosynthetic activity in plants, and reproductive development and locomotion in the roundworm *Caenorhabditis elegans* (*C. elegans*) (van der Linden et al., 2010). Finally, ultradian rhythms occur with a period of less than 24 hours, such as the beating of the human heart and gut peristalsis. Regardless of the period time associated with a particular behavior, all rhythmic behaviors are controlled by a biological clock referred to as a pacemaker. The pacemaker is responsible for maintaining the rhythmicity of the behavior, which in turn maintains proper physiological functioning. Investigating the molecular mechanisms responsible for establishing and maintaining pacemaker activity is necessary for a more complete understanding of how rhythmic behaviors such as heart beat, breathing, sleeping, and gut peristalsis, to name a few, are regulated.

Mammalian gut peristalsis is an ultradian rhythmic behavior

Peristalsis of the gastrointestinal (GI) tract in humans and other animals is an example of an ultradian rhythmic behavior. Ultradian rhythmic behaviors are regulated by pacemakers, which are individual cells or groups of cells that establish and maintain rhythmicity of the behavior. Propagation of peristaltic contractions is achieved through slow-wave pacemaker activity (Huizinga et al., 2009). Slow waves are defined as

spontaneous electrical activity in the pace-making units of the GI tract that are then propagated to neighboring pace-making units and smooth muscle cells (Sanders et al., 2006, Huizinga et al., 2009).

The pace-making units for human gut peristalsis are interstitial cells of Cajal (ICC). ICC are able to generate rhythmic, electrical slow-waves in the absence of external stimuli from nerves, hormones, or paracrine signals and are able to maintain this rhythmicity for up to three days in culture (Ward et al., 2000, Sanders et al., 2006). ICC form large complexes connected to each other and to smooth muscle cells via gap junctions (Komuro et al., 2006). To control the rhythmic contractions of GI smooth muscle cells, the ICC and smooth muscle cells are electrically coupled; meaning depolarization events occurring in the ICC are translated to the smooth muscle cells to cause contraction (Sanders et al., 2006, Huizinga et al., 2009).

The pacemaker activity of ICC is regulated by fluctuations of intracellular calcium (Ca^{2+}) concentrations. Ca^{2+} enters the ICC through voltage-dependent, nonselective cation channels and T-type Ca^{2+} channels (Huizinga et al., 2009, Zhu et al., 2015). Fluctuations in membrane potential seem to be the initiating factor for Ca^{2+} influx into ICC, however the mechanism(s) responsible for changes in membrane potential remain unknown (Zhu et al., 2015). Blocking voltage-dependent entry of Ca^{2+} into ICC inhibits the propagation of slow-waves, and subsequent muscle contractions (Sanders et al., 2006). Although there have been no direct measurements of localized Ca^{2+} influx into ICC to confirm the role of Ca^{2+} in activating the slow-waves characteristic of pacemaker activity, inhibiting Ca^{2+} entry into ICC has the effect of abolishing slow-waves (Zhu et al., 2015).

The current model for ICC pacemaker activity implicates the role of microdomains. Electron microscopy of isolated ICC showed that microdomains exist between the plasma membrane and the endoplasmic reticulum (ER), which may act as the "pacemaker unit" for ICC pacemaker activity (Rumessen et al., 1993, Zhu et al., 2015). Local changes in Ca^{2+} concentration, due to Ca^{2+} influx, could result in Ca^{2+}-induced Ca^{2+} release (CICR) (Zhu et al., 2015). Alternatively, the local influx of Ca^{2+} into microdomains activates the Ca^{2+}-activated Cl^- channel (CaCC), ANO1 (Zhu et al., 2015). However, there have been no successful measurements of Ca^{2+} "sparks" or "puffs" within microdomains, so little is known about Ca^{2+} dynamics within pacemaker microdomains (Zhu et al., 2015).

One potential model for ICC pacemaker activity is as follows: local Ca^{2+} influx into microdomains activates CaCC, resulting in a spontaneous transient inward current (STICs) (Zhu et al., 2015). STICs cause cell depolarization, which leads to whole-cell Ca^{2+} entry, CICR, IP_3 production, or some combination of those events (Zhu et al. 2015). Finally, the synchronized intracellular Ca^{2+} influx resulting from cell depolarization can be propagated through the ICC network (Zhu et al., 2015).

It is possible that the influx of Ca^{2+} into the ICC results in the activation of phospholipase C (PLC) which converts the membrane phospholipid phosphatidylinositol 4,5-bisphosphate (PIP_2) into the second messenger inositol 1,4,5-trisphosphate (IP_3). IP_3 then activates the IP_3-receptor (IP_3R) on the sarco/endoplasmic reticulum, inducing the release of Ca^{2+} from intracellular stores (Huizinga et al., 2009). Ca^{2+} release from intracellular stores, such as the sarco/endoplasmic reticulum and mitochondria, is linked to the initiation of slow-waves, which is the characteristic activity of pacemaker cells

(Ward et al., 2000, Sanders et al., 2006). Visualization of intracellular Ca^{2+} in ICC shows that Ca^{2+} influx into the ICC network occurs "nearly" simultaneously with the propagation of anal-directed slow-waves (Huizinga et al., 2009).

Input from the ICC is required for the rhythmic coordination of smooth muscle contractions that are characteristic of GI peristalsis, since GI smooth muscle cells are unable to generate and propagate slow-waves (Sanders et al., 2006). Without the input of ICC pacemaker activity, coordinated contraction of the GI smooth muscle cells is lost (Sanders et al., 2006). Therefore, loss of ICC pacemaker activity is implicated in various gastrointestinal diseases, such as gastroparesis, pseudo-obstruction, chronic constipation, and posttraumatic/post-infectious dysfunction (Sanders et al., 2006).

The *C. elegans* intestine: development and physiology

The intestine is one of the major organs in *C. elegans,* comprising roughly one-third of the somatic mass of the organism (McGhee, 2007) (Figure 1A). The intestine is responsible for digestion of ingested bacteria, absorption of nutrients, and defecation (Altun et al., 2009). All 20 epithelial cells of the intestine originate from a single progenitor cell, the E blastomere (Altun et al., 2009) (Figure 1B). At the 8-cell embryonic stage, the E blastomere divides into anterior- (Ea) and posterior- (Ep) E cells (Altun et al., 2009). These two cells, Ea and Ep, further divide into Ea left and right, and Ep left and right, and migrate to the interior of the embryo (Altun et al., 2009). Further divisions of Ea left and right, and Ep left and right result in 16 primordial intestinal cells positioned in two tiers (McGhee, 2007). Lastly, the anterior cell pair and posterior cell pair divide to produce the 20 intestinal cells that make up the adult intestine (Altun et al.,

2009). At this point, the primordial intestinal cells become polarized and fuse with one another in order to form the intestinal lumen. The two semi-circular intestinal cells are joined together by adherens junctions on the apical cell side (Altun et al., 2009, McGhee, 2007). Each set of intestinal cells is referred to as an int, with nine ints comprising the *C. elegans* intestine (Figure 2). Int1 is composed of four fused intestinal cells, while int2 through int9 are composed of two fused intestinal cells (McGhee, 2007). Each int is connected to neighboring ints via gap junctions on the lateral cell side (Altun et al., 2009, McGhee, 2007). Ultimately, the ints form a bilaterally symmetrical, single-cell layer that makes up and surrounds the intestinal lumen (Altun et al., 2009).

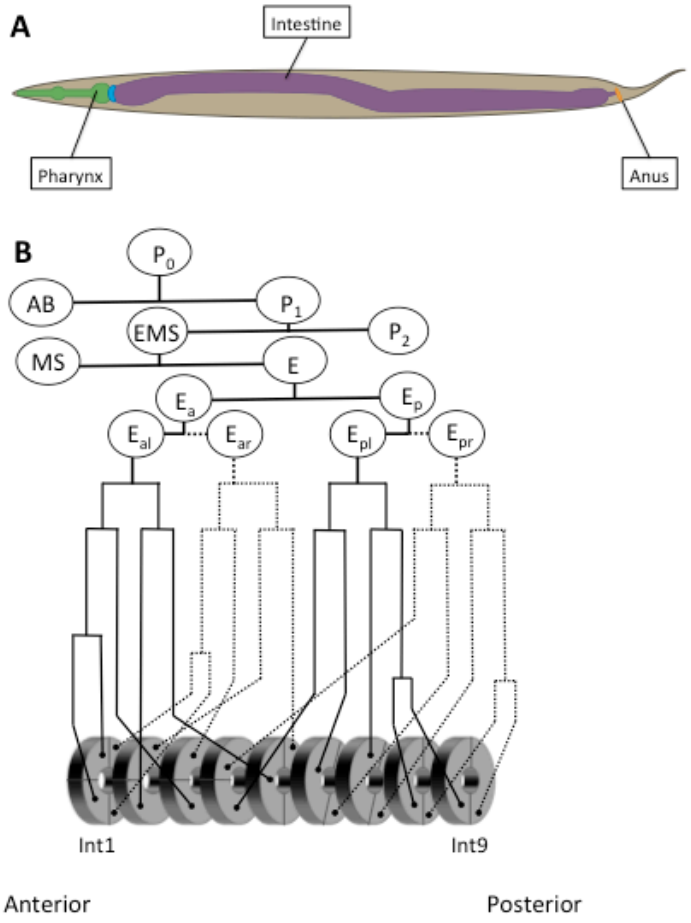

Figure 1. The *C. elegans* Intestine.
A. An illustration of the *C. elegans* intestine. B. A schematic representation of the embryonic cell lineage of the *C. elegans* intestine.

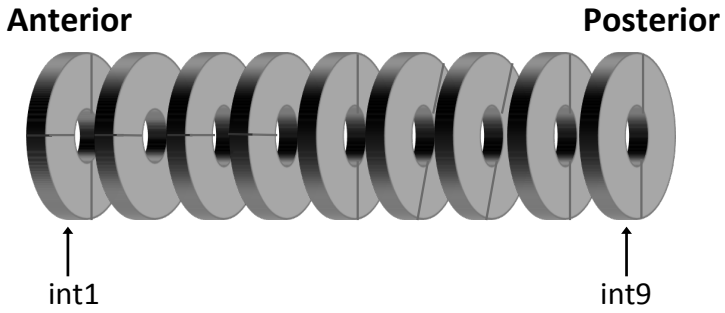

Figure 2. *C. elegans* Intestinal Cells.
A graphic representation of the 9 intestinal rings (ints) of the *C. elegans* intestine. Modified from Kemp et al., 2012.

Although the *C. elegans* intestine may appear to be a simple, single-layered tube, the ints are patterned to perform different functions. As noted previously, the *C. elegans* intestine in responsible for digestion, nutrient absorption, and expulsion of waste. In order to perform these various functions, the ints are specialized to accomplish these tasks. For example, the cells in int1 and int2 have shorter microvilli than the more posterior ints, presumable for digestion in int1 and int2 and absorption of nutrient in the more posterior ints (McGhee, 2007). Int9, the most posterior int, acts as the pacemaker for the defecation motor program (DMP) (McGhee, 2007). Also, genes required for pacemaker function are either exclusively expressed in the posterior intestinal cells of int9 or are expressed to a higher degree in int9 than other intestinal ints (Dal Santo et al., 1999) Int9 will be referred to as the pacemaker cell.

The structures relevant to the DMP that are located in the hindgut include int9, the anus, non-striated body wall muscles, and two GABAergic motor neurons, AVL and DVB (Altun et al., 2009) (Figure 3). The non-striated stomatointestinal muscles associated with the intestine (also referred to as posterior body wall muscles) connect the intestine surface to the body wall (Altun et al., 2009) (Figure 3). The posterior body

muscles are electrically coupled to the two enteric muscles necessary for defecation, the anal sphincter and anal depressor muscles, via gap junctions (Altun et al., 2009). The anal sphincter muscle and anal depressor muscle are also innervated by the two GABAergic neurons, AVL and DVB (Altun et al., 2009) (Figure 3).

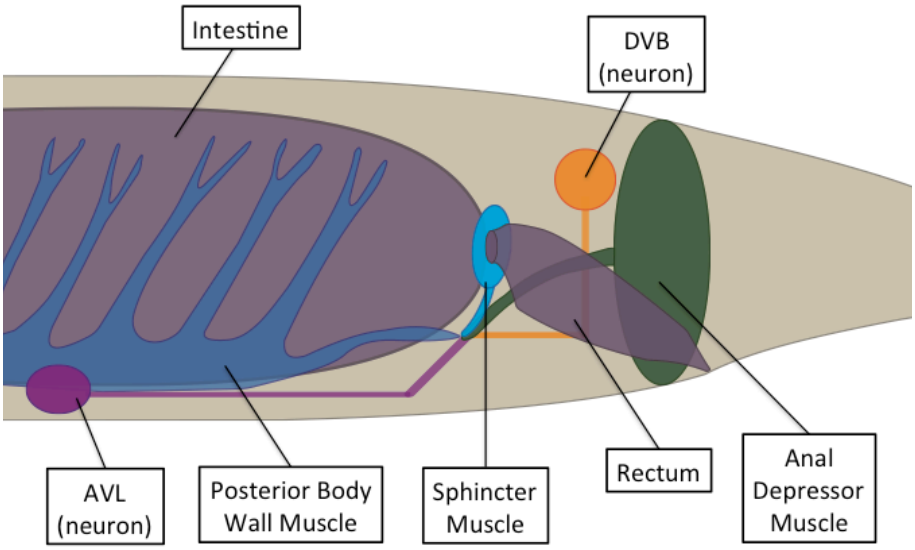

Figure 3. *C. elegans* Posterior Intestinal Structures.
An illustration of the muscles and neurons in the posterior intestine that are relevant to the DMP.

The *C. elegans* Defecation Motor Program is an ultradian rhythmic behavior

The *C. elegans* intestine is responsible for digestion, absorption of nutrients, and defecation. The process of defecation is an example of an ultradian rhythm that is tightly regulated by pacemaker activity. The defecation motor program (DMP) is one of three well-characterized ultradian rhythmic behaviors observed in *C. elegans*: pharyngeal pumping, ovulation, and defecation. Similar to human GI peristalsis, the DMP in *C. elegans* requires a specialized pacemaker unit to establish and maintain rhythmic muscle contractions. Defects in the DMP result in severely constipated worms. The *C. elegans*

DMP comprises three sequential muscle contractions: a posterior body contraction (pBoc), followed by an anterior body contraction (aBoc), and finally an enteric muscle contraction (EMC) coupled to the expulsion of waste (Exp) (Dal Santo, 1999) (Figure 4). A defecation cycle is defined as the time interval between two consecutive pBocs (Branicky et al., 2006). In wild-type worms, the pBoc occurs every ~45 seconds in response to intracellular Ca^{2+} spikes. The elevation of Ca^{2+} in the posterior intestine initiates a Ca^{2+} wave that propagates through the intestine in the anterior direction, which is necessary for the normal execution of the aBoc and Exp steps of the DMP (Dal Santo et al., 1999, Peters et al., 2007).

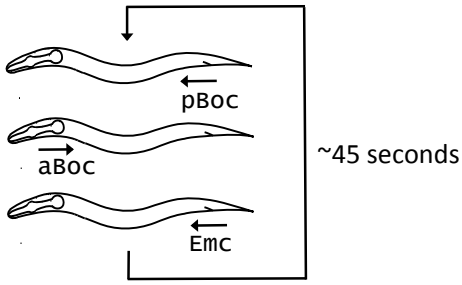

Figure 4. The Defecation Motor Program.
An illustration depicting the three characteristic muscle contraction of the DMP: pBoc, followed by aBoc, and finally Emc coupled to Exp.

The DMP can be modulated by various environmental stimuli, such as mechanical stimulation, feeding, and temperature. Mechanical stimulation, such as light touch, resets the defecation cycle resulting in a longer interval between pBocs (Branicky et al., 2006). Feeding also has the ability to modulate the DMP. Decreased food concentration results in increased cycle lengths (Branicky et al., 2006). However, no correlation between pharyngeal pumping rate and defecation rate has been identified, so it seems unlikely that a feedback loop exists between pumping and defecation (Branicky et al., 2006). Another interesting feature of the defecation cycle is temperature compensation. Wild-type worms

use a temperature compensation mechanism to keep cycle lengths the same across varying temperatures, a characteristic consistent with the requirements of an ultradian rhythm (Branicky et al., 2006). However, mutants with dysfunctional temperature compensation mechanisms display altered cycle lengths when exposed to higher or lower temperatures (Branicky et al., 2006). For example, shifting mutant worms from 20°C to 15°C results in longer cycle lengths, while shifting from 20°C to 25°C results in shorter cycle lengths (Branicky et al., 2006).

The DMP is a Ca^{2+}-dependent rhythmic behavior, meaning that fluctuations in intracellular Ca^{2+} concentration control the rhythmicity of the behavior. Intracellular Ca^{2+} elevation in the posterior intestine, the pacemaker, is propagated to subsequent intestinal cells as a Ca^{2+} wave that moves in the posterior to anterior direction. Posterior-to-anterior wave propagation is positively correlated with the successful execution of the entire DMP: pBoc, aBoc, and EMC/Exp (Nehrke et al., 2008, Peters et al., 2007).

The first contraction of the DMP is the pBoc, in which the posterior body muscles contract in the anterior direction, pushing waste toward the anterior intestine (Dal Santo et al., 1999). The posterior body wall muscle contraction is initiated by an elevation of intracellular Ca^{2+} in int9, the pacemaker (Dal Santo et al., 1999). The pBoc does not require neuronal input, but rather depends on the elevation of intracellular Ca^{2+} concentration for initiation (Dal Santo et al., 1999). Similar to cultured ICC cells from the mammalian GI tract, dissected *C. elegans* intestines are able to execute rhythmic Ca^{2+} waves for up to 18 hours after dissection, highlighting the autonomous nature of pBoc initiation (Teramoto et al., 2006).

Following the pBoc is the aBoc, in which the anterior body wall muscle cells contract in the posterior direction. This contraction pressurizes waste at the posterior intestine near the anus, in preparation for expulsion (Iwasaki et al., 1995). The aBoc occurs when the Ca^{2+} wave initiated in the posterior intestine, reaches the anterior intestine (Teramoto et al., 2006). Unlike the pBoc, in which no neuronal input is required for contraction, the aBoc requires two GABAergic neurons AVL and DVB for contraction. Although the molecular mechanism of the aBoc has not been determined it likely utilizes a similar molecular pathway as Exp (Branicky et al., 2006). This contraction occurs approximately 3 seconds after the pBoc, when cytoplasmic Ca^{2+} in the anterior cells returns to normal levels (Teramoto et al., 2006, Nehrke et al., 2008).

Finally, after completion of the pBoc and aBoc contractions, specialized enteric muscles contract to expel the waste contents from the anus (Iwasaki et al., 1995). Similar to the aBoc step, the enteric muscle contraction and expulsion steps require neuronal input from the AVL and DVB neurons (Branicky et al., 2006). Exp is initiated by the release of a neuropeptide, NLP-40, from the intestine into the pseudocoelom (Wang et al., PLoS, 2013). NLP-40, encoded by *nlp-40,* is expressed exclusively in the intestine. In response to elevated intracellular Ca^{2+}, the Ca^{2+} sensor SNT-2, a synaptotagmin family member, elicits the release of NLP-40 through exocytosis (Wang et al., Current Biology, 2013). After release into the pseudocoelom, NLP-40 binds to, and subsequently activates the G-protein coupled receptor (GPCR), AEX-2, located on DVB (Wang et al., 2013). Activation of AEX-2/GPCR results in the downstream activation of adenylyl cyclase, which produces the 2° messenger, cAMP (Wang et al., PLoS, 2013). Increased levels of cAMP activate the protein kinase A (PKA) homolog KIN-1, which leads to robust Ca^{2+}

influx through voltage-gated Ca^{2+} channels, such as UNC-2 and EGL-2, and possibly non-voltage-dependent Ca^{2+} channels (Wang et al., PLoS, 2013). Using a Ca^{2+} indicator expressed exclusively in the DVB neuron, researchers observed a single, robust Ca^{2+} spike in the synaptic region of the DVB approximately 3 seconds after the pBoc, immediately prior to Exp (Wang et al., Current Biology, 2013). The influx of Ca^{2+} as a result of KIN-1 activation occurs either through direct phosphorylation of the Ca^{2+} channels, or through KIN-1-mediated regulation of membrane potential (Wang et al., PLoS, 2013). Depolarization of the GABAergic neuron, through Ca^{2+} influx, results in the release of the neurotransmitter GABA (Wang et al., Current Biology, 2013). GABA then binds to the excitatory receptor, EXP-1, located on the enteric muscle, to cause enteric muscle contraction and expulsion of waste (Wang et al., Current Biology, 2013).

Worms with mutations in the components of this pathway display defective defecation cycles. For example, worms with mutations in *nlp-40* display distended intestinal lumens indicative of constipation, significantly reduced Exp, and reductions in aBoc (Wang et al., Current Biology, 2013). Similarly, worms with mutations in the Ca^{2+} sensor gene, *snt-2*, phenocopy the defects seen in *nlp-40* mutant worms (Wang et al., Current Biology, 2013). This observation indicates that the neuropeptide, NLP-40, released from the intestine is required for proper execution of the Exp step of the DMP. Additionally, mutations in the receptor, *aex-2*, phenocopy the constipation, loss of Exp, and defect in aBoc seen in *nlp-40* mutants (Wang et al., Current Biology, 2013).

The rhythmicity of the DMP is regulated by pacemaker activity

Initiation of the DMP is regulated by rhythmic influx of Ca^{2+} into int9, at the posterior intestine. Ca^{2+} elevation in the pacemaker cell is then propagated toward the anterior intestine as an intracellular Ca^{2+} wave (Branicky et al., 2006). The Ca^{2+} wave moves from the posterior intestine to anterior intestine at a speed of 340 ± 140 μm/s via gap junctions (Teramoto et al., 2006, McGhee et al., 2007). However, the exact molecule moving through gap junctions has not been determined. It is possible that IP_3 moves through the gap junctions to initiate Ca^{2+} release, or that Ca^{2+} moves through the gap junctions to increase the intracellular Ca^{2+} concentration of subsequent ints, or both (Peters et al., 2007).

Ca^{2+} wave propagation is abnormal when components of the gap junctions are defective (Teramoto et al., 2006, Peters et al., 2007). The frequency and velocity of the Ca^{2+} wave is also regulated by an IP_3R, ITR-1, found on the endoplasmic reticulum (Branicky et al., 2006). Intracellular Ca^{2+} levels peak immediately prior to the initiation of pBoc (Branicky et al., 2006). Ca^{2+} increase in one int, starting at int9, leads to muscle contraction in the muscle overlying that region of the intestine, resulting in a sequential contraction of the posterior body wall muscle (Peters et al., 2007). This is described as a point-to-point intestinal cell to muscle cell signal transduction (Peters et al., 2007).

Both the site of initiation at the posterior intestine and the posterior-to-anterior direction of propagation of Ca^{2+} waves are necessary for proper execution of the DMP. All intestinal cells are capable of initiating Ca^{2+} waves, however, only waves that originate in the posterior intestine and move toward the anterior intestine are capable of initiating the full DMP (Nehrke et al., 2008). Ectopic initiation of Ca^{2+} waves—from

either the anterior intestine or middle intestine—moving in the posterior direction are not able to elicit normal aBoc or Exp contractions (Nehrke et al., 2008).

The site of Ca^{2+}-wave initiation is regulated, in part, by proteins localized to gap junctions, EGL-8 and INX-16 (Nehrke et al., 2008, Peters et al., 2007). EGL-8 encodes a *C. elegans* phospholipase Cβ (PLCβ) ortholog, which is localized at gap junctions and at neuromuscular junctions (Nehrke et al., 2008). In *egl-8(n488)* mutant worms, arrhythmic and ectopic Ca^{2+} waves are observed (Nehrke et al., 2008). *egl-8* mutants display random Ca^{2+} oscillations, with equal probability of Ca^{2+} wave initiation occurring at the anterior-, posterior-, or mid-intestine (Nehrke et al., 2008). Although expression of *egl-8* occurs throughout the intestine, the highest expression level is observed in the posterior intestine, indicating the role of EGL-8 in reinforcing the supremacy of int9 as the pacemaker cell for defecation (Nehrke et al., 2008). Interestingly, EGL-8 displays increased activity in response to elevated intracellular Ca^{2+} levels (Nehrke et al., 2008). This may indicate that EGL-8 affects the defecation cycle by regulating membrane cation channels indirectly through depletion of the membrane lipid, PIP_2. It is known that high PIP_2 levels inhibit membrane cation channels, so depletion of PIP_2 via EGL-8 activity could activate membrane cation channels, a characteristic required for Ca^{2+} wave initiation and propagation (Xing et al., 2009). However, the function of EGL-8 in relation to regulation of the DMP remains unknown (Xing et al., 2009).

Another gap junction protein responsible for regulating the site of Ca^{2+} wave initiation is INX-16. INX-16 is exclusively localized to sites of cell contact between ints (Peters et al., 2007). *inx-16* mutants display constipation, slow growth, decreased brood size, and have a smaller adult body size than wild-type worms (Peters et al., 2007). Using

a genetically encoded Ca^{2+} sensor to visualize the Ca^{2+} dynamics in *inx-16* mutant worms, three main phenotypes were observed (Peters et al., 2007). First, propagation of a Ca^{2+} wave was not observed in 21% of the mutants analyzed; the posterior cell had a Ca^{2+} spike, but no wave resulted (Peters et al., 2007). Second, when a Ca^{2+} wave was observed, it had a reduced velocity (Peters et al., 2007). Finally, in over 50% of the mutants displaying Ca^{2+} waves, the wave was initiated ectopically (Peters et al., 2007). Ca^{2+} waves beginning in the mid-intestine spread outward in both directions and failed to elicit the aBoc and Exp steps of the DMP (Peters et al., 2007). Together, these data indicate that INX-16 is also responsible for maintaining the superiority of int9 as the pacemaker cell for the DMP.

Ca^{2+} enters the pacemaker cell through TRP channel homologs

Ca^{2+} elevation observed in the DMP requires two Transient Receptor Potential (TRP) channels (Teramoto et al., 2005). TRP channels are a superfamily of non-selective, mono- and bivalent cation channels (Kahn-Kirby et al., 2006). The superfamily of TRP channels contains 7 subfamilies, all of which are represented in the *C. elegans* genome; these are categorized based on sequence similarity and include TRPC, TRPM, TRPML, TRPP, TRPN, TRPA, and TRPV (Kahn-Kirby et al., 2006). TRPs assemble into homo- and heterotetramers to form functional cation-selective channels (Kahn-Kirby et al., 2006). In *C. elegans*, TRP channels are involved in olfaction, mechanosensation, and osmosensation (Kahn-Kirby et al., 2006). TRP channels can be regulated by multiple pathways: thermal stimuli, mechanical stimuli, lipids or lipid derivatives, voltage, pH, phosphorylation, and most interestingly to the process of defecation, intracellular Ca^{2+}

concentration and levels of the membrane lipid PIP_2 (Kahn-Kirby et al., 2006, Gees et al., 2010, and Xing et al., 2010).

The TRP channels specific to the process of defecation in *C. elegans* are two TRPM (melastatin) channel homologs (Kahn-Kirby et al., 2006). TRPM channels have 6 predicted transmembrane segments, with N- and C-terminal tails both residing on the cytoplasmic side of the membrane (Fleig et al., 2004). The *C. elegans* genome encodes three TRPM homolog channels, *gtl-1, gtl-2,* and *gon-2* (Kwan et al., 2008). Using promoter fusion proteins, it was shown that *gtl-1* and *gon-2* are expressed in the intestine, while *gtl-2* is expressed in the excretory cell (Teramoto et al., 2005). Low intracellular Ca^{2+} concentrations have been shown to activate both GON-2 and GTL-1 (Xing et al., 2010). Additionally, Xing et al., (2010) demonstrated that GON-2 and GTL-1 are regulated by PIP_2 levels, in which high levels of PIP_2 inhibit channel activity and low levels of PIP_2 stimulate channel activity. Worms with mutations in either of these channel genes display slow-growth phenotypes, and have long and irregular defecation cycles (Teramoto et al., 2005). Both channels are required for generating intestinal Ca^{2+} oscillations (Xing et al., 2010). Interestingly, *dec-11* worms also display the slow-growth phenotype.

The IP_3 pathway mediates intracellular Ca^{2+} release

Entrance of Ca^{2+} into the pacemaker cell via GON-2 and GTL-1 is proposed to activate Ca^{2+} release via the IP_3 pathway (Xing et al., 2010). The *C. elegans* PLCγ homolog, PLC-3, is activated by the entry of Ca^{2+} through GON-2 and GTL-1, although the molecular interaction eliciting this activity is unknown (Xing et al., 2010). PLCγ

generates IP_3 through cleavage of PIP_2 (Xing et al., 2010) (Figure 5A). IP_3 then binds to ITR-1 located on the surface of the endoplasmic reticulum, which stimulates the release of Ca^{2+} from this intracellular store (Dal Santo et al., 1999) (Figure 5A). The endoplasmic reticulum is the major IP_3-sensitive intracellular Ca^{2+} store in *C. elegans* (Taylor et al., 2012).

ITR-1 is biphasically regulated by IP_3 and Ca^{2+} levels. Upon binding of IP_3 to ITR-1, low levels of intracellular Ca^{2+} concentrations activate the receptor to release stored Ca^{2+} (Taylor et al., 2012). Conversely, high levels of intracellular Ca^{2+} inhibit ITR-1-mediated Ca^{2+} release (Taylor et al., 2012). In *C. elegans* ITR-1 is required for defecation cycle timing, by regulating the intracellular Ca^{2+} concentration in the pacemaker cell (Dal Santo et al., 1999). ITR-1 generates increased intracellular Ca^{2+} concentrations in the intestinal cytoplasm and therefore controls pBoc cycle times (Dal Santo et al., 1999). *itr-1* loss-of-function mutations result in slowed or absent Ca^{2+} oscillations which correlate with irregular or absent defecation cycles, while ITR-1 overexpression results in shortened defecation cycle lengths (Branicky et al., 2006).

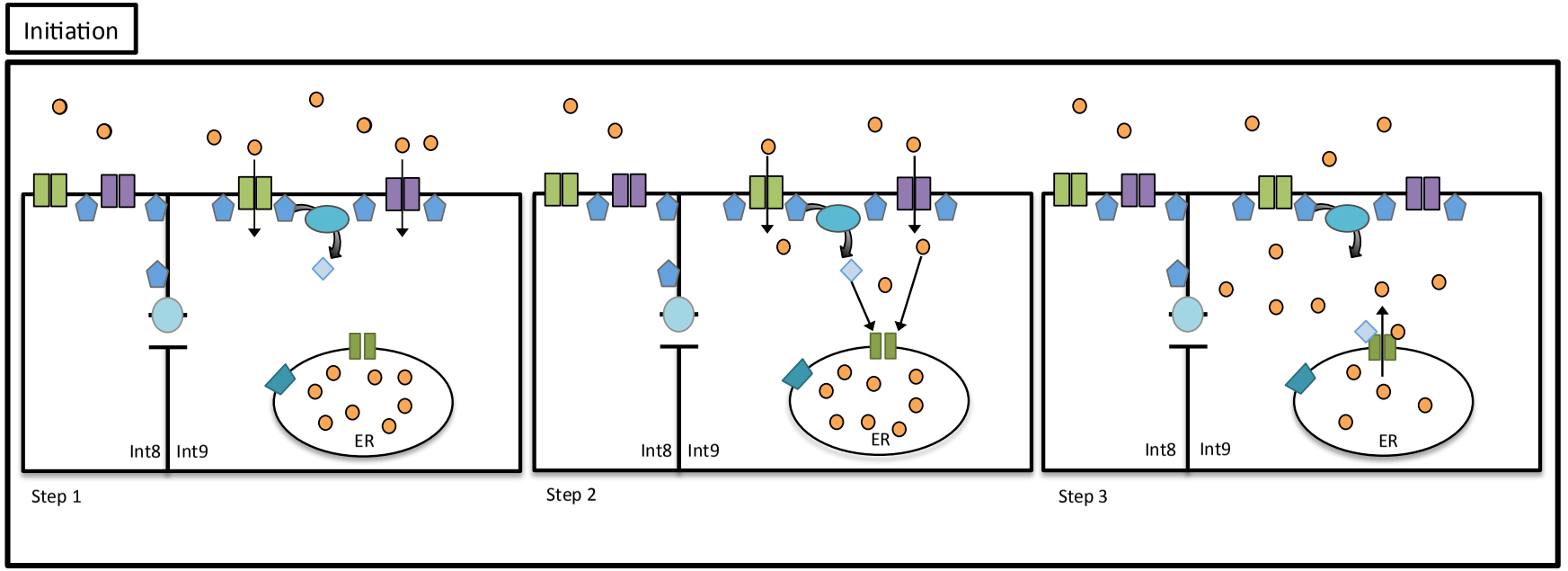

Figure 5A. Pacemaker Activity in the *C. elegans* DMP.
A. The steps necessary for the initiation of the DMP: Step 1. Ca^{2+} enters the pacemaker cell through two TRPM channel homologs, GON-2 and GTL-1. The influx of Ca^{2+} activates PLCγ, which converts PIP_2 into IP_3. Step 2. IP_3 and high levels of intracellular Ca^{2+} activate ITR-1 on the surface of the endoplasmic reticulum (ER). Step 3. Activation of ITR-1 results in the release of stored intracellular Ca^{2+}, further increasing intracellular Ca^{2+} levels.

A Na^+/H^+ exchanger acidifies the pseudocoelom to activate muscle contraction

Fluctuations in intracellular Ca^{2+} concentration have also been shown to positively and negatively regulate various Na^+/H^+ exchangers (Allman et al., 2013). Pfeiffer et al. (2008) identified a high affinity Calmodulin (CaM)-binding site on the C-terminus of NHX-7, a *C. elegans* Na^+/H^+ exchanger, encoded by *pbo-4* (Beg et al. 2008). NHX-7 is located on the basolateral plasma membrane of posterior intestinal cells (Beg et al., 2008). When NHX-7 becomes activated, likely by increased intracellular Ca^{2+} concentration, it pumps H^+ ions from the intestinal cytoplasm into the extracellular space between the intestine and the muscle (Allman et al., 2013) (Figure 5B). The acidification of the pseudocoelom, through increased concentration of H^+ ions, activates PBO-5/6, a ligand-gated cation channel, located on the posterior body muscle membrane (Allman et al., 2013) (Figure 5B). Activation of PBO-5/6 through binding of H^+ ions, results in muscle-cell depolarization and pBoc (Beg et al., 2008, Allman et al., 2013). Acidification of the pseudocoelom persists approximately 3 seconds, which is generally correlated to the length of the pBoc (Pfeiffer et al., 2008).

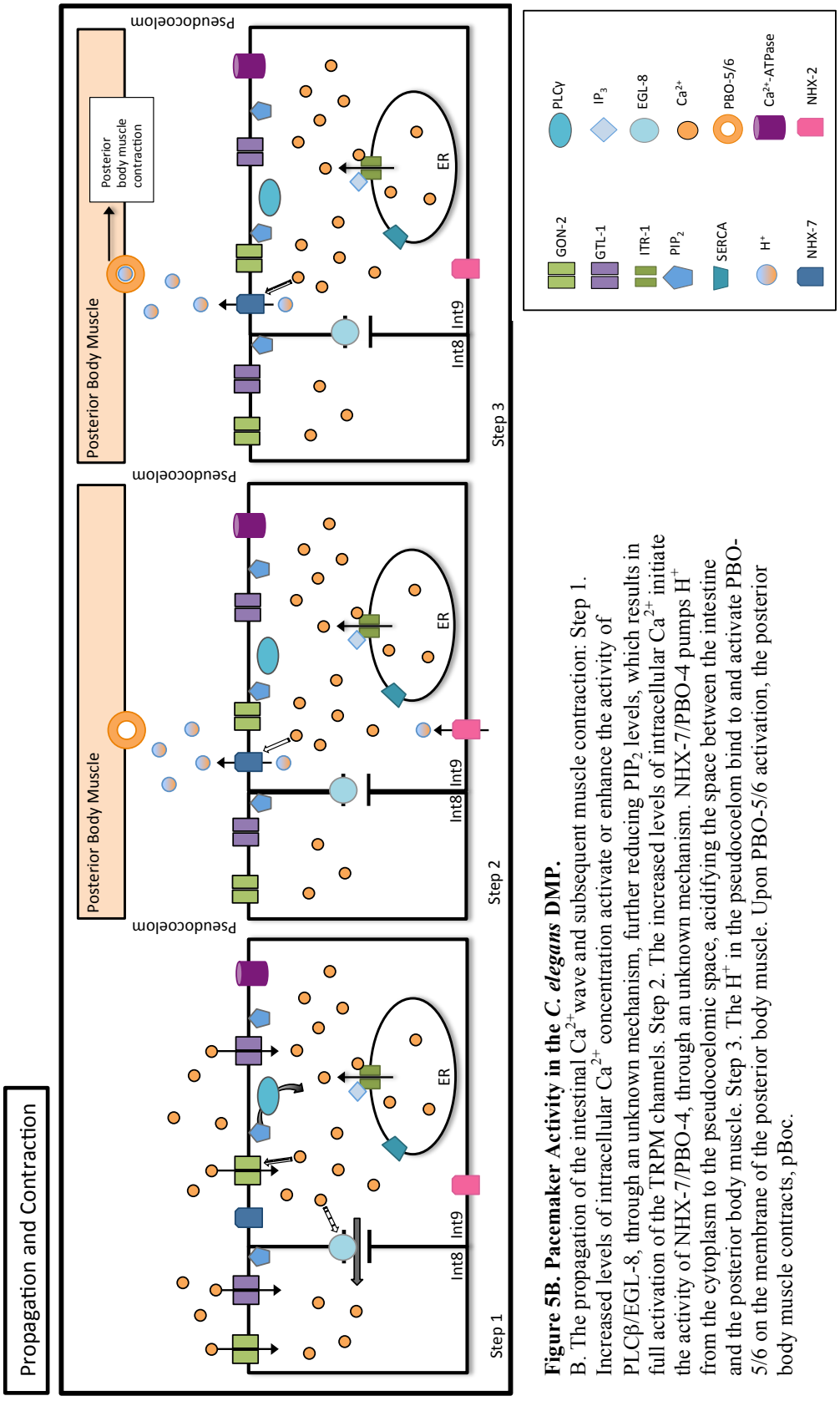

Figure 5B. Pacemaker Activity in the *C. elegans* DMP.
B. The propagation of the intestinal Ca^{2+}wave and subsequent muscle contraction: Step 1. Increased levels of intracellular Ca^{2+} concentration activate or enhance the activity of PLCβ/EGL-8, through an unknown mechanism, further reducing PIP_2 levels, which results in full activation of the TRPM channels. Step 2. The increased levels of intracellular Ca^{2+} initiate the activity of NHX-7/PBO-4, through an unknown mechanism. NHX-7/PBO-4 pumps H^+ from the cytoplasm to the pseudocoelomic space, acidifying the space between the intestine and the posterior body muscle. Step 3. The H^+ in the pseudocoelom bind to and activate PBO-5/6 on the membrane of the posterior body muscle. Upon PBO-5/6 activation, the posterior body muscle contracts, pBoc.

Another Na^+/H^+ exchanger necessary for the DMP, NHX-2, is located on the apical membrane of the intestinal cells facing the intestinal lumen (Pfeiffer et al., 2008). NHX-2 is responsible for the normal flow of H^+ between the intestinal lumen and intestinal cytoplasm (Pfeiffer et al., 2008). The intestinal lumen has a resting pH of approximately 4.1 in wild-type worms (Pfeiffer et al., 2008). The pH of the intestinal lumen rises dramatically immediately prior to initiation of the pBoc, to approximately 6.0 due to the activity of NHX-2 pumping H^+ from the lumen into the cytoplasm (Pfeiffer et al., 2008). NHX-7 can then pump H^+ from the cytoplasm to the pseudocoelom to activate PBO-5/6.

Another interesting characteristic regarding the interaction between intracellular Ca^{2+} concentration and pH levels is the regulation of gap junctions. It is known that both Ca^{2+} and pH play a role in gating gap junction (Pfeiffer et al., 2008). It is possible that increased intracellular Ca^{2+} levels and the resulting decrease in cytoplasmic pH allows for H^+ to gate the gap junctions found at each int, in order to prevent "cellular metabolites"—such as IP_3, Ca^{2+}, or other 2° messengers—from flowing backwards through the intestine (Pfeiffer et al., 2008). Therefore, H^+-gating of the gap junctions could be responsible, in part, for shaping the intestinal Ca^{2+} wave in the posterior to anterior direction.

Intracellular Ca^{2+} concentration returns to baseline after completion of the DMP

After completion of the DMP, intracellular Ca^{2+} must return to baseline, in order to prepare the cells for the execution of subsequent defecation cycles. Membrane Ca^{2+}-ATPases are responsible for removing a portion of the intracellular Ca^{2+}, while sarco/endoplasmic reticulum Ca^{2+}-ATPases (SERCAs) located on the sarco/endoplasmic

reticulum membrane are responsible for refilling the intracellular Ca^{2+} store (Nehrke et al., 2008) (Figure 5C). Both mechanisms are required for returning intracellular Ca^{2+} concentration to baseline. In *C. elegans,* SERCA is encoded by *sca-1* (Nehrke et al., 2008). Intestine-specific, RNAi knock-down of *sca-1* resulted in worms that were unable to defecate and displayed no rhythmic Ca^{2+} oscillations (Nehrke et al., 2008). Additionally, the length of time in which intracellular Ca^{2+} levels were elevated, was significantly increased in the *sca-1*(RNAi) worms when compared to control worms (Nehrke et al., 2008). This observation is consistent with the role of SERCA in refilling the sarco/endoplasmic reticulum with cytoplasmic Ca^{2+}.

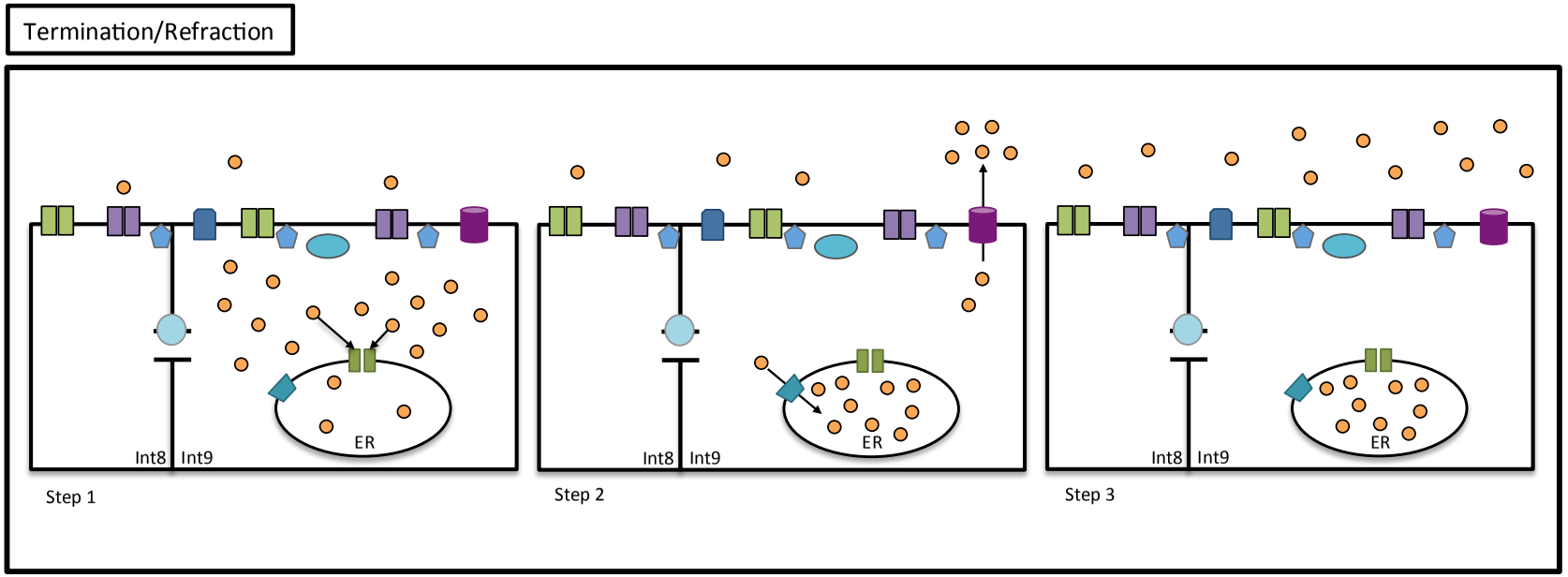

Figure 5C. Pacemaker Activity in the *C. elegans* DMP.
C. The termination of Ca^{2+} signaling in the pacemaker cell and subsequent refractory period: Step 1. High levels of intracellular Ca^{2+} inhibit ITR-1 activity, thus inhibiting the further release of Ca^{2+} from the ER. Step 2. SERCA is activated and begins to pump cytoplasmic Ca^{2+} back into the ER, to replenish the intracellular store. Concomitantly, Ca^{2+}-ATPase on the plasma membrane pumps cytoplasmic Ca^{2+} into the extracellular space. Step 3. The pacemaker cell remains inactive until the next defecation cycle is initiated by the influx of Ca^{2+} through GON-2 and GTL-1.

As intracellular Ca^{2+} levels return to baseline, the pacemaker cell enters into a "refractory" period, in which it is incapable of initiating the DMP. CaM and Calcium/CaM-dependent serine/threonine kinase type II (CaMKII) become activated in response to heightened intracellular Ca^{2+} levels. CaM and CaMKII are responsible for establishing and maintaining the refractory period. In *C. elegans*, CaMKII is encoded by *unc-43*, the only CaMKII encoded in the *C. elegans* genome (Nehrke et al., 2008). UNC-43 is expressed in muscles, neurons, and the intestine and is activated by Ca^{2+}-CaM (Reiner et al., 1999). *unc-43* loss-of-function mutants display a "shadow" DMP, or weak repetition of the DMP, approximately 10 seconds after the previous DMP (Nehrke et al., 2008, Reiner et al., 1999). Ca^{2+} waves that occur during the "shadow" contraction are indistinguishable from the Ca^{2+} waves that occur immediately prior to the normal DMP execution (Nehrke et al., 2008). In 85% of mutants, *unc-43* gain-of-function mutant worms display loss of the expulsion step, and long and irregular defecation cycles (Nehrke et al., 2008). Based on this data, it is believed that CaMKII functions to suppress a predicted plasma "membrane pacemaker", a pace-making unit that oscillates much faster than the observed DMP period (Nehrke et al., 2008). A CaMKII loss-of-function mutation abolishes the ability of CaMKII to inhibit the oscillations of the membrane pacemaker, which results in "shadow" DMPs (Nehrke et al., 2008). This may occur through CaMKII inhibition of ITR-1 activity (Nehrke et al., 2008).

In summary, *C. elegans* utilizes a multitude of proteins and pathways to properly regulate the DMP. A current model to account for the rhythmicity of the Ca^{2+} dependent DMP is the following: extracellular Ca^{2+} enters the pacemaker cell, at the posterior intestine, through two TRPM channel homologs GON-2 and GTL-1. The influx of Ca^{2+}

stimulates PLCγ activity, producing the second messenger IP_3. IP_3 is then responsible for the robust activation of ITR-1, on the endoplasmic reticulum membrane, and subsequent release of intracellular Ca^{2+} stores into the cytosol. The increase of intracellular Ca^{2+} in the posterior intestine is propagated in the anterior direction through gap junctions, resulting in an increase in intracellular Ca^{2+} concentration in all intestinal cells. Proper location and direction of intracellular Ca^{2+} spikes is regulated, in part, by the activity of gap-junction proteins EGL-8 and INX-16. Elevations in intracellular Ca^{2+} result in activation of the Na^+/H^+ exchanger NHX-7 and subsequent release of H^+ ions into the pseudocoelom. Acidification of the extracellular space between the intestine and the posterior body muscle activates PBO-5/6 to induce muscle cell depolarization and pBoc. Upon arrival of the Ca^{2+} wave at the anterior end of intestine, the two excitatory GABAergic neurons AVL and DVB are activated resulting in the aBoc and EMC/Exp steps of the DMP. Once a DMP has been completed, it is then necessary for intracellular Ca^{2+} to return to baseline, in order to prepare the cells for the next defecation cycle. This is accomplished through the activity of both plasma membrane Ca^{2+}-ATPases and SERCA. The activity of CaMKII maintains the refractory period until the pacemaker cell is ready to initiate another defecation cycle.

A forward genetic screen identifies genes required for normal DMP pacemaker activity

To identify genes that regulate the execution of the DMP, Iwasaki et al. performed a forward genetic screen (1995). One of the mutants identified, *dec-11(sa292)*, is classified as a dec-l mutant, because of the long defecation cycle phenotype in these mutants. *dec-11(sa292)* displays long and irregular defecation cycles when compared to

wild-type worms, indicating that *dec-11* mutants lack normal pacemaker activity (Iwasaki, 1995). The mutation in *dec-11* results in multiple phenotypes. As mentioned previously, *dec-11* mutant worms lack defecation pacemaker activity, a phenotype that is exacerbated at high temperatures. When cultured and scored at 25°C, *dec-11(sa292)* mutants display longer defecation cycles, with an average cycle length between 60 and 90+ seconds (Iwasaki et al., 1995). Additionally, *dec-11* mutants exhibit a slow-growth phenotype when compared to wild-type worms (Iwasaki et al., 1995). However *dec-11(sa292)*, the gene that is mutated in *dec-11* worms remains unknown. Previously published genetic mapping data indicates that *dec-11* is located on the right arm of chromosome IV, at 12.36 ± 3.77 cM, a region containing roughly three million base pairs (Iwasaki, 1995).

In order to more fully understand the molecular role of *dec-11* in regulating defecation pacemaker activity, we sought to identify how *dec-11* is involved in the regulation of DMP pacemaker activity, and to identify the gene that is mutated. Using genetic analysis, single nucleotide polymorphism (SNP) interval mapping, and whole-genome sequencing (WGS), we sought to identify the gene mutated in *dec-11(sa292)* worms and the role *dec-11* plays in maintaining pacemaker activity.

II. RESULTS: GENETIC AND FUNCTIONAL ANALYSIS OF dec-11

Characterization of *dec-11* defecation phenotype

The DMP is characterized by three distinct muscle contractions: pBoc, aBoc, and Emc. Defecation cycles are defined as the time interval between two consecutive pBocs. In wild-type worms, this behavior occurs every 45 seconds ± 1.09 seconds (Figure 6A). To characterize the defecation phenotypes associated with a mutation in the gene *dec-11*, the defecation cycles of *dec-11* mutant worms were scored. The defecation cycles observed in *dec-11* mutant worms are significantly longer and irregular in comparison to wild-type worms (Figure 6B and C).

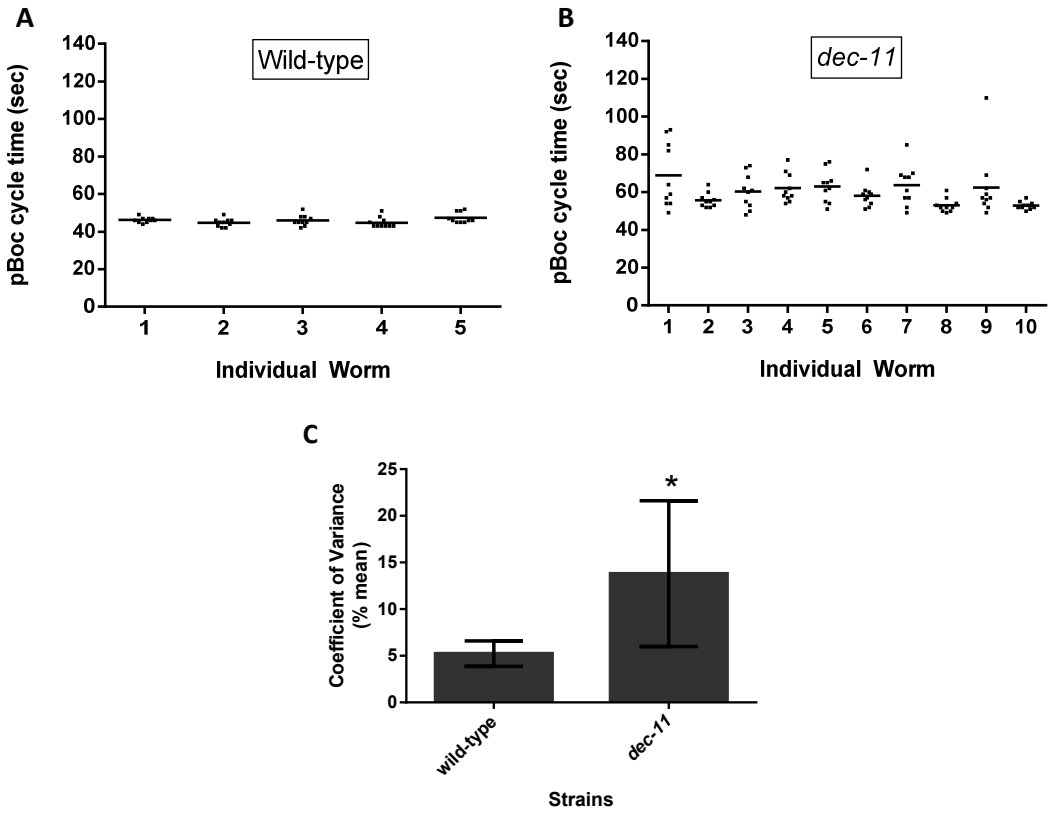

Figure 6. *dec-11* is necessary for normal DMP-pacemaker activity.
Defecation analysis of the defecation cycle times in wild-type (A) or *dec-11* (B) individual worms. Individual cycle times are represented by dots, with the mean represented as a solid line. Ten defection cycles were analyzed for each worm. p<.01 by a two-tailed t-test (C) The average coefficient of variance for the defecation cycles of wild-type and *dec-11* worms. *p<.01 by a two-tailed t-test

To further characterize the defecation phenotypes of *dec-11* mutant worms, video microscopy was used. It has been shown that irregular pacemaker activity, such as arrhythmic Ca^{2+} signaling, can result in irregular muscle twitching between pBocs. For example, *miR240/786* mutant worms display shadow pBocs as a result of ectopic Ca^{2+} signaling (Kemp et al., 2012). Although monitoring pBocs can be readily performed in real time, the subsequent steps occur too quickly to be simultaneously monitored. Video microscopy allows us to capture the DMPs in wild-type and mutant worms and more closely analyze the execution of the steps in the DMP, thereby allowing us to identify any subtle or weak irregularities that may occur between the three characteristic muscle contractions in *dec-11* worms. As seen previously, video microscopy allows for the identification of any abnormalities in the defecation behavior, such as contractions that occur between cycles (Kemp et al., 2012).

Video microscopy data from the *dec-11* mutant worms revealed that once initiated, the DMP proceeds normally (Table 1). There were no irregular contractions observed outside of the three characterized contractions of the DMP: pBoc, aBoc, and expulsion. The irregularity of the DMP initiation was observed in the video microscopy data. Thus, the long, irregular defecation cycles in *dec-11* mutants are likely due to defects in the initiation or refraction step of the DMP and not the subsequent steps. Furthermore, the data suggest that there are not defects in ectopic Ca^{2+} elevation or wave propagation in the *dec-11* mutant worms. To confirm this conclusion, Ca^{2+} visualization is necessary.

Table 1. Video Microscopy Data Summary

genotype	Average time pBoc-pBoc (sec)	SD	Average time pBoc-aBoc (sec)	SD	Average time pBoc-Exp (sec)	SD	% aBoc failure	% Exp failure	number of worms	number of cycles
wild-type	52.5	4.2	4.0	0.5	4.3	0.5	0	0	7	78
dec-11	59.1[a]	12.44	3.2	0.4	3.9	0.3	2	1	10	96

[a] two-tailed t-test analysis, different from wild-type, $p < .01$

dec-11 functions upstream of, or in parallel to, ITR-1-Mediated Ca^{2+} release

ITR-1-mediated Ca^{2+} release occurs downstream of Ca^{2+} influx into the pacemaker cell (Xing et al., 2010). Epistasis analysis was performed to determine if *dec-11* functions upstream or downstream of ITR-1-mediated Ca^{2+} release using *ipp-5* and *lfe-2* loss-of-function mutations. Loss of *ipp-5* or *lfe2* activity, an IP_3 phosphatase and an IP_3 kinase respectively, results in higher levels of IP_3 due to the reduced conversion of IP_3 to IP_2 or IP_4, respectively (Figure 7A). Loss of either *ipp-5* or *lfe-2* activity was found to suppress defects in the molecular pathway of pacemaker activity that occur upstream of ITR-1-mediated Ca^{2+} release (Kemp et al., 2012). We hypothesized that if *dec-11* works upstream of, or in parallel to, ITR-1-mediated Ca^{2+} release, mutations in *ipp-5* or *lfe-2* would suppress the *dec-11* mutant phenotype. In agreement with this hypothesis we found that loss of *ipp-5* or *lfe-2* was able to partially suppress the mutant defecation phenotype of *dec-11* worms (Figure 7B and C). This data indicates that *dec-11* likely works upstream of, or in parallel to, ITR-1-mediated Ca^{2+} release.

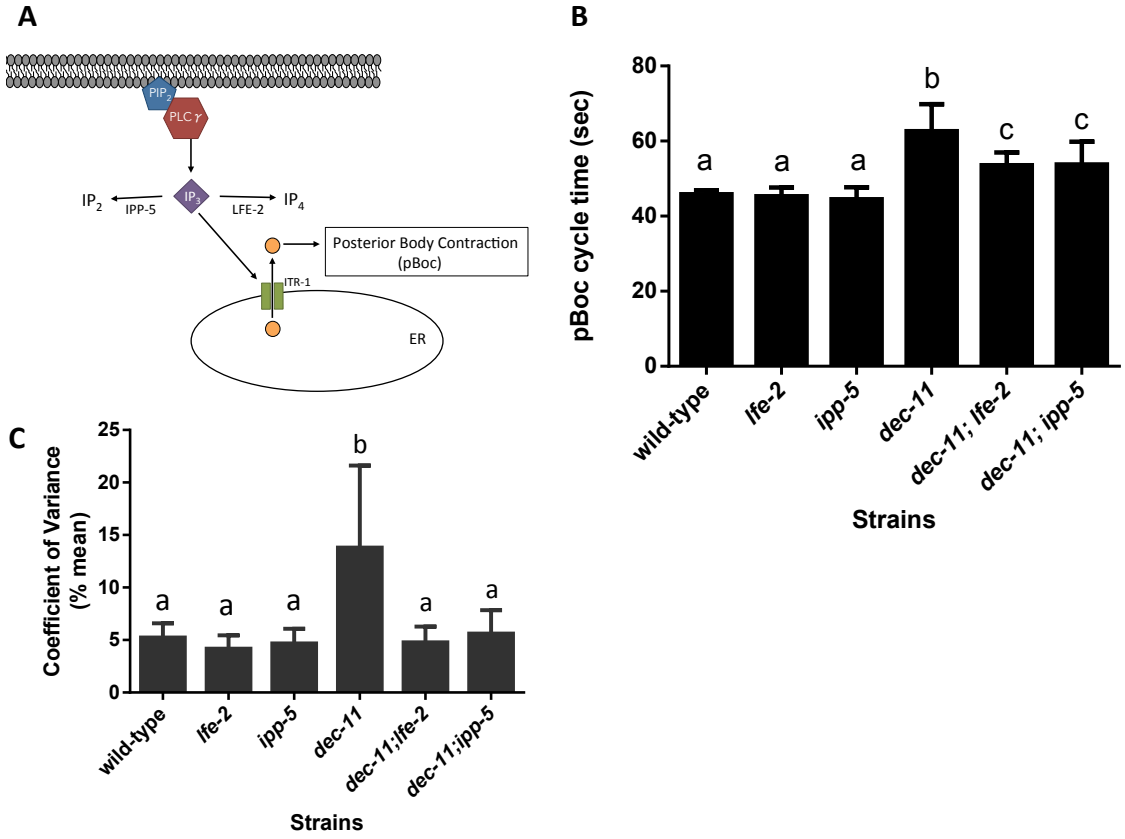

Figure 7. Increased levels of IP_3 suppress the *dec-11* phenotype.
(A) IP_3-mediated pathway of intracellular Ca^{2+} release: hydrolysis of the membrane lipid PIP_2 by PLCγ, generates the second messenger IP_3. IP_3 then binds to ITR-1, on the surface of the ER, resulting in the release of stored Ca^{2+}. IP_3 can be converted to IP_4 by LFE-2, an IP_3 kinase, or to IP_2 by IPP-5, an IP_3 phosphatase. (B) Bars represent the average of averages from the defection analysis of 10 defecation cycles per 10 individual worms. Means with different letters indicate statistically significant differences. $p < .01$ by One-way ANOVA (C) The average coefficient of variance was calculated for five to ten worms for each strain. Means with different letters indicate statistically significant differences. $p < .01$ by One-way ANOVA

High Mg^{2+} suppresses the *dec-11* defecation phenotype upstream, or in parallel to, GON-2/GTL-1 activity

Ca^{2+} influx into the pacemaker cell, through two TRPM channels GON-2 and GTL-1, initiates the DMP. Previously published data demonstrate that loss-of-function mutations in either of these genes, *gon-2* and/or *gtl-1,* results in long and irregular defecation cycles, since they are required for initiation of the DMP (Teramoto et al., 2005). Since GON-2 and GTL-1 are non-selective bivalent cation channels, Teramoto et al. (2005) analyzed the defecation cycles of *gon-2* and/or *gtl-1* mutant worms on high and low Mg^{2+} and Ca^{2+} plates. They observed that the long and irregular defecation cycles observed in the mutants could be suppressed by supplementing growth plates with high Mg^{2+}, but not Ca^{2+} (Teramoto et al., 2005). Teramoto et al. (2005) conclude that *gon-2* and *gtl-1* mutations alter the physiological state of the intestine, which can be rectified by supplementing the growth media with high Mg^{2+}. They also conclude that the defective DMP observed in *gon-2*, *gtl-1* mutants is the result of Mg^{2+} deficiency, since high Mg^{2+} but not high Ca^{2+} was able to restore rhythmic defecation cycles (Teramoto et al., 2005).

Based on epistatic data placing the function of *dec-11* upstream of, or in parallel to, ITR-1-mediated Ca^{2+} release, the long and irregular defecation cycles observed in *dec-11* mutants, and the data published by Teramoto et al. (2005), we hypothesized that *dec-11* mutants cultured on plates containing high Mg^{2+} would have a suppressed mutant defecation phenotype. Consistent with our hypothesis, growth on high Mg^{2+} plates resulted in significant suppression of the *dec-11* defecation phenotype (Figure 8C and D). The defecation cycles of wild-type worms grown on high (40mM) Mg^{2+} was not significantly different than wild-type worms grown on normal (1mM) Mg^{2+} plates (Figure 8A and B). Suppression of the *dec-11* mutant phenotype by supplementation with

high Mg^{2+} indicates that *dec-11* may alter the physiological state of the intestine, rather than a developmental defect. Additionally, since high Mg^{2+} has been shown to restore rhythmicity to *gon-2*, *gtl-1* mutants (Teramoto et al., 2005), it is possible that *dec-11* also functions to regulate initiation or refraction of the DMP.

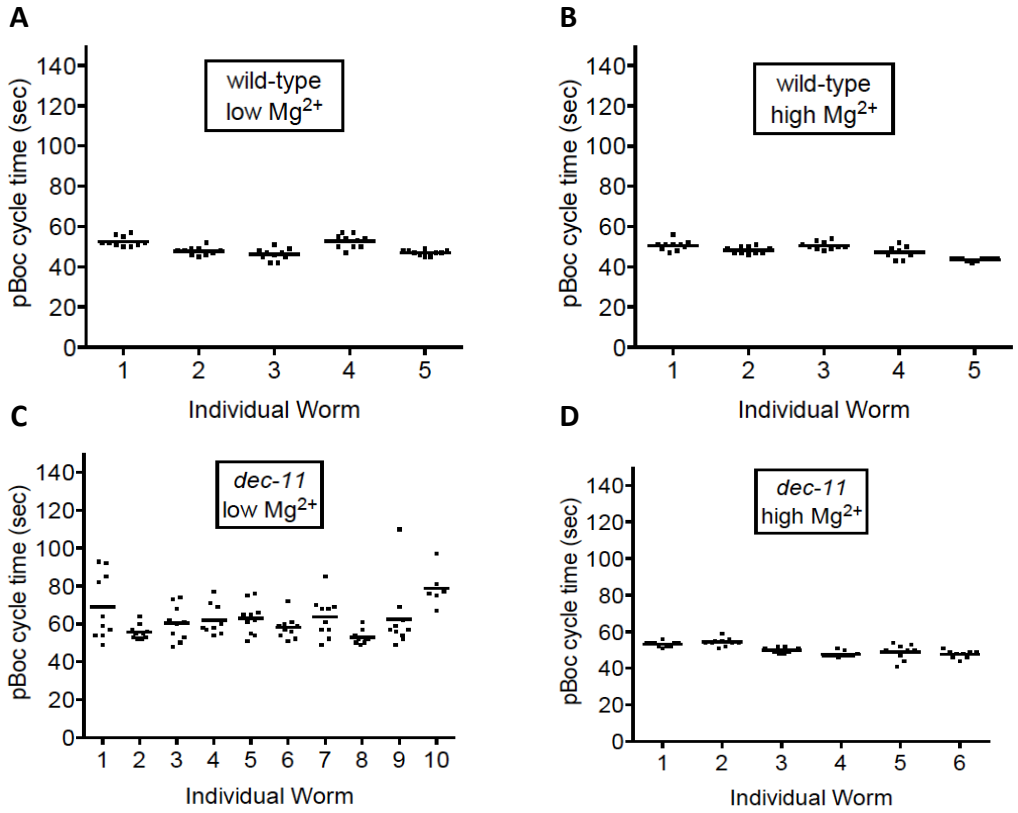

Figure 8. Effects of Mg^{2+} concentrations on the DMP.
The defecation cycles of individual worms were analyzed on either low (1mM) or high (40mM) Mg^{2+} NGM plates. 10 defecation cycles were analyzed for each worm represented by dots, means are represented by a solid line. High Mg2+ rescued defects in the *dec-11* mutants. p< .01 by a two-tailed t-test.

Since the DMP is a Ca^{2+}-dependent behavior, and TRPM channels allow for the passage of both Ca^{2+} and Mg^{2+}, we also tested the effect of high Ca^{2+} on *dec-11* mutant worms. Unlike the suppression observed with high Mg^{2+}, *dec-11* worms cultured on high Ca^{2+} growth medium continued to display long and irregular defecation cycles, which is consistent with the data published by Teramoto et al., 2005 (Figure 9C and D). Wild-type worms grown on high Ca^{2+} plates also displayed significantly longer and irregular cycles (Figure 9A and B). Since TRPM channels are permeable to both Mg^{2+} and Ca^{2+} (Harteneck, 2005), it is possible that increasing extracellular Ca^{2+} levels allows for the preferential passage of Ca^{2+} into the cell, resulting in irregular defecation cycles. It is equally possible that increased extracellular Ca^{2+} affects the ability of cells to pump Ca^{2+} out of the cytoplasm to return intracellular Ca^{2+} concentrations to baseline resulting in longer intervals between pBocs.

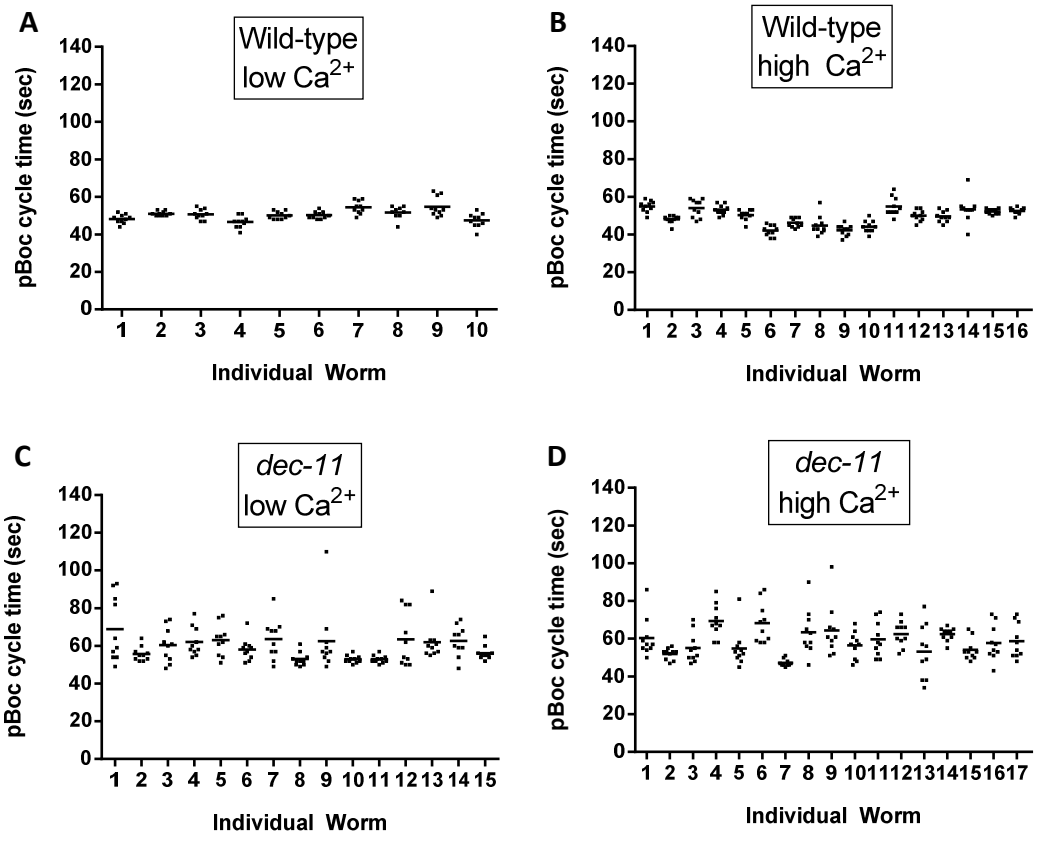

Figure 9. Effects of Ca^{2+} concentration on the DMP.
The defecation cycles of individual worms were analyzed on either low (1mM) or high (5mM) Ca^{2+} NGM plates. 10 defecation cycles were analyzed per individual worm, represented as dots. The mean is represented as a solid line. High Ca^{2+} did not rescue the *dec-11* mutant phenotype.

III. RESULTS: *dec-11* MOLECULAR ANALYSIS

In parallel to the genetic analysis of *dec-11* mutant worms, we performed molecular mapping using SNP interval mapping, RNAi analysis, and WGS to identify the gene that is mutated in *dec-11* worms. Previously published genetic mapping places *dec-11* at 12.37 ± 3.77 centiMorgans (cMs) on the right arm of chromosome IV, a region containing roughly 2 million base pairs and over 223 candidate genes (Iwasaki et al., 1995).

SNP Interval Mapping refines the genetic interval in which *dec-11* is located

In order to identify the molecular location of *dec-11*, we performed SNP interval mapping using the protocol published by Davis et al. (2005). *dec-11* hermaphrodites, which have a Bristol (N2) isolate background, were mated to Hawaiian isolate males (CB4956), to generate progeny heterozygous at each SNP (Figure 10). In this way, SNPs from the mutant Bristol genome and SNPs from the Hawaiian reference strain can be identified for analysis of recombination events based on the presence or absence of a restriction enzyme site. Recombination events in the F2 progeny, in the region that is in close proximity (linked) to the *dec-11* mutation will be unlikely, therefore a high percentage of Bristol SNPs will remain around *dec-11*, with no Hawaiian SNPs observed in this region (Figure 10).

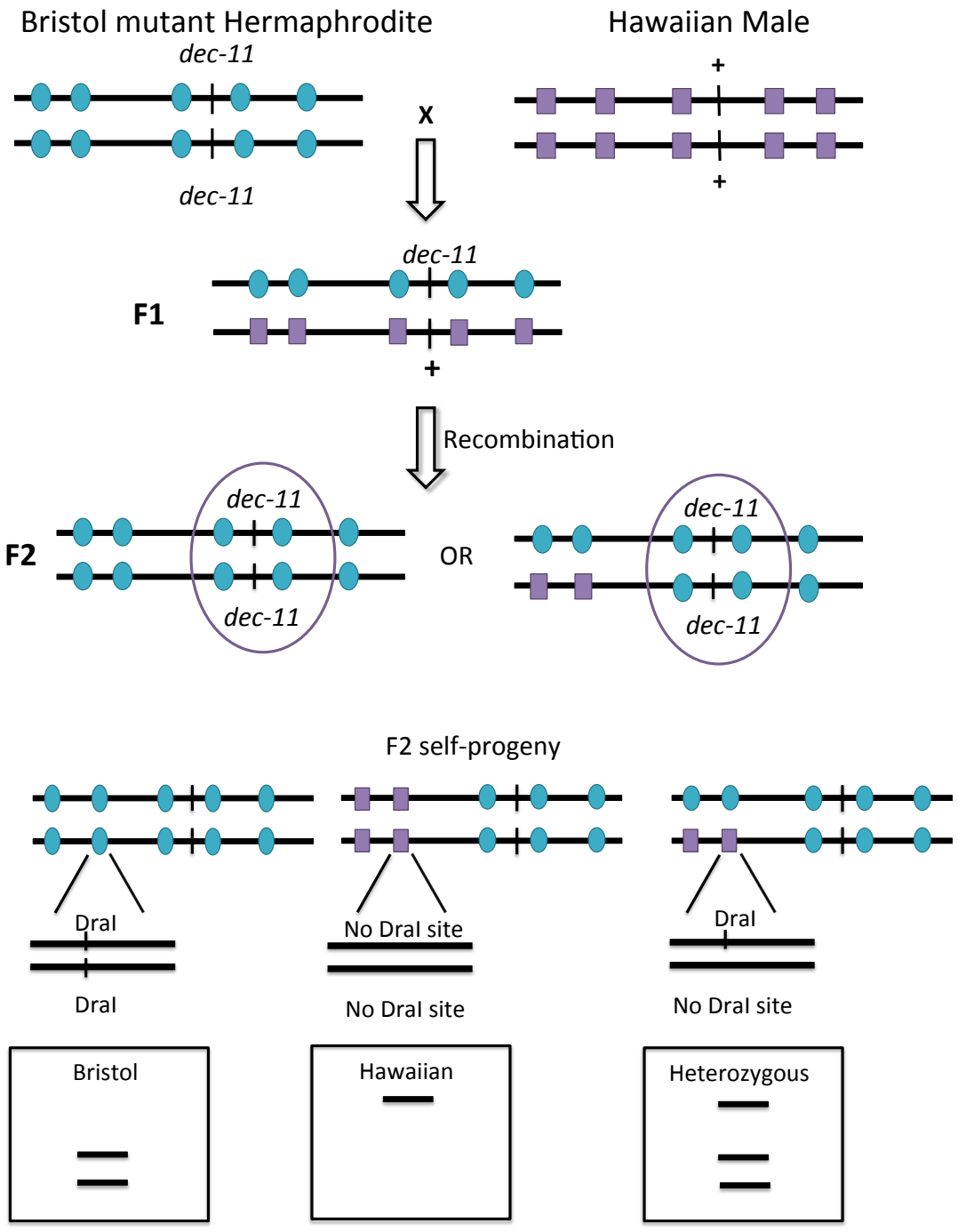

Figure 10. Principle of the SNP Interval Mapping Strategy.
Aqua ovals represent a Bristol (N2) variant SNP, while purple squares represent a Hawaiian (CB4856) variant SNP. DNA can be digested with the restriction enzyme DraI to determine the SNP composition at a particular SNP.

Analysis of SNPs on the right arm of chromosome IV identified a refined interval containing approximately 698, 518 base pairs and 62 candidate genes. Further SNP mapping is limited by the small number of confirmed Hawaiian and Bristol SNPs in this region of the chromosome. The left and right boundaries of this interval are tentatively located at nucleotides 15,321,502 and 16,020,020 on the right arm of chromosome IV, based on data points with n≥3. This interval theoretically contains the genetic region in which *dec-11* most likely exists (Figure 11). Using this interval, we prioritized a candidate gene list containing protein-coding, pseudogenes, and non-coding RNAs (ncRNA) (Table 2). Candidate genes were prioritized based on their availability in either of the two RNAi libraries, Ahringer and Vidal. Candidate genes with a known function, that were not present in either library, were analyzed next by constructing RNAi plasmids. 21UR genes were excluded from the candidate list.

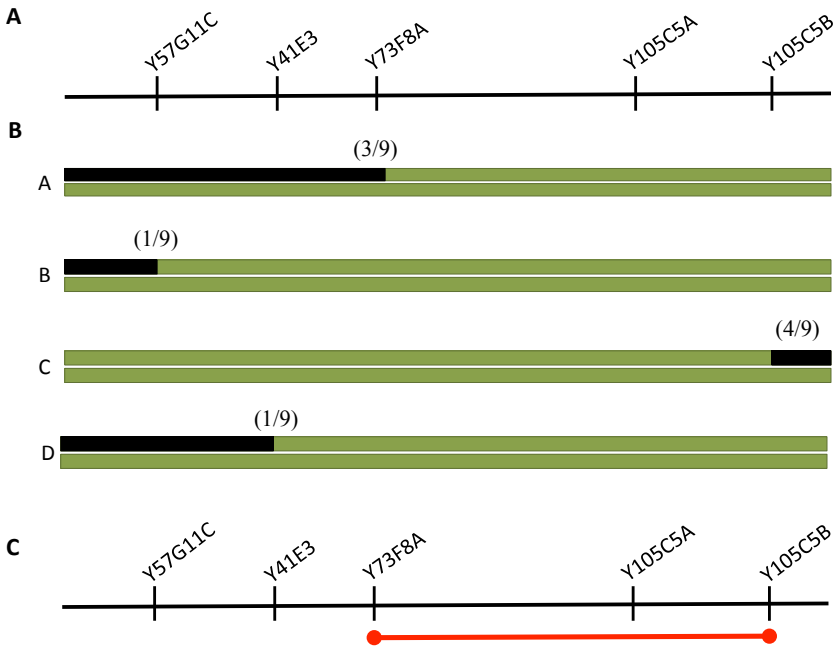

Figure 11. SNP Interval Mapping on the right arm of Chromosome IV.
(A) SNPs analyzed on the right arm of chromosome IV. B. Data from SNP interval mapping is summarized in (B), which shows the recombinant phenotypes of the 9 worms tested. Black denotes a Hawaiian variant SNP, while green denotes a Bristol variant SNP. (C) The red line represents the interval containing *dec-11*.

Table 2. *dec-11* Candidate Gene List

Gene Name	Gene ID	Gene Description
	Y73F8A.15*	
tbx-39	Y73F8A.16*	T BoX family, expressed in intestine ("patchy")
tbx-40	Y73F8A.17*	T BoX family (single neuron)
irld-59	Y73F8A.18	
cpna-4	Y73F8A.19*	
	Y73F8A.20*	
	Y73F8A.1159	
nhr-5	Y73F8A.21	*C. elegans* nuclear receptor
	Y73F8A.22*	
	Y73F8A.23*	
	Y73F8A.24*	
ntl-11	Y73F8A.25*	
	Y73F8A.27	
	Y73F8A.26*	
acr-24	Y73F8A.30*	Nicotinic acetylcholine receptor
	Y73F8A.32*	
	Y73F8A.33	
tag-349	Y73F8A.34*	
	Y73F8A.35	
	Y105C5A.1*	
pqn-76	Y105C5A.3	
	Y105C5A.508	
abu-5	Y105C5A.4*	Transmembrane protein may function within the ER to protect the organism from damage by improperly folded nascent protein.
pqn-78	Y105C5A.5*	
pqn-79	Y105C5A.6	
	Y105C5A.8	
	Y105C5A.9*	
	Y105C5A.1274*	
	Y105C5A.10*	
srg-19	Y105C5A.11*	Serpentine Receptor
	Y105C5A.13*	
	Y105C5A.12*	
	Y105C5A.1268	
	Y105C5A.1272*	
	Y105C5A.26*	
	Y105C5A.15*	
	Y105C5A.17	
	Y105C5A.1285	
	Y105C5A.1273	
	Y105C5A.22	
daf-38	Y105C5A.23*	G-protein coupled receptor
	Y105C5A.1270*	
	Y105C5A.1269	
	Y105C5A.24	
	Y105C5B.1	
gcy-25	Y105C5B.2*	Predicted guanylate cyclase.
	Y105C5B.3	

Table 2. *dec-11* Candidate Gene List, *continued*

srv-14	Y105C5B.4*	Serpentine Receptor
	Y105C5B.5*	
srv-15	Y105C5B.6*	Serpentine Receptor
	Y105C5B.8*	
	Y105C5B.9*	
srv-16	Y105C5B.10*	Serpentine Receptor
	Y105C5B.11*	
skr-10	Y105C5B.13*	homolog of Skp1 in *S. cerevisiae*
	Y105C5B.14*	
	Y105C5B.15*	
lgc-19	Y105C5B.16	Ligand-Gated ion Channel
	Y105C5B.17*	
	Y105C5B.18*	
	Y105C5B.19*	
	Y105C5B.20*	

*Genes analyzed by RNAi

RNAi analysis of candidate genes identified by SNP-mapping failed to identify *dec-11*

Based on the results of SNP interval mapping, we sought to identify *dec-11* by RNAi analysis of the candidate genes identified in the tentative interval between base pairs 15,321,502 and 16,020,020 (Table 2). We hypothesized that RNAi knockdown of the gene corresponding to *dec-11* would phenocopy the long and irregular defecation cycles observed in *dec-11* mutants. Of the 40 candidate genes analyzed by RNAi, none phenocopied the *dec-11* mutant phenotype (Figure 12). RNAi analysis of candidate genes was discontinued based on the decision to pursue WGS. We decided that using WGS would provide a faster and more accurate identification of the phenotype-causing mutation in *dec-11* worms.

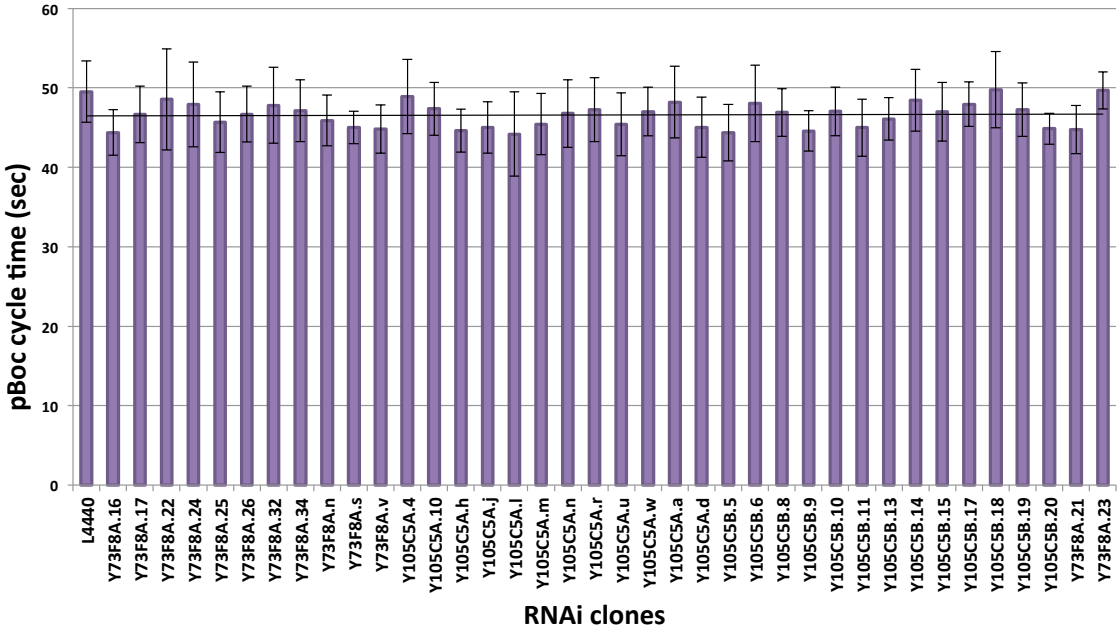

Figure 12. Knockdown of *dec-11* candidate genes by RNAi did not phenocopy the *dec-11* mutant phenotype. 20 individual worms per candidate gene RNAi clone were analyzed for 10 defecation cycles. Bars represent the average of average defecation cycle times for each RNAi clone. L4440 is empty RNAi vector, used as a control.

Whole-Genome Sequencing identifies *dec-11* candidate genes

In parallel to SNP mapping and RNAi analysis of candidate genes, we performed WGS on a DNA sample that represented pools of progeny isolated from a cross between *dec-11* mutants and the Hawaiian mapping strain (CB4856) (Doitsidou et al., 2010). This technique allows for precise SNP mapping and gene-variant identification, since mutagenized strains often have a significant number of genetic variations that are not linked to the mutant phenotype. By generating a recombinant population, we will be able to use recombination frequency to refine the interval containing *dec-11* to a very specific region, further allowing us to identify the phenotype-causing mutation (Doitsidou et al., 2010). To do this, Hawaiian isolate males (CB4856) were mated to *dec-11* mutant hermaphrodites in a Bristol background, to generate F1 progeny that were heterozygous

at each SNP. F1 worms were then allowed to self-fertilize to generate recombinant F2 progeny (Figure 13). The WGS results can then be analyzed using the automated workflow, CloudMap, a cloud-based workflow used to analyze mutant genome sequences (Minevich et al., 2012).

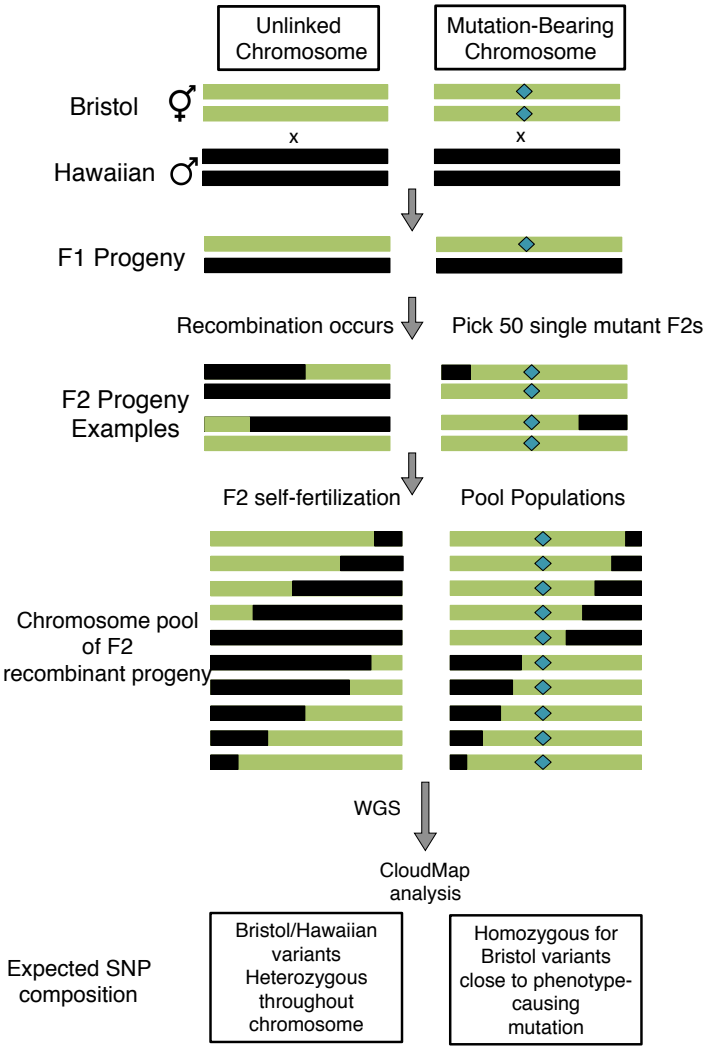

Figure 13. Principle of the WGS Strategy.
dec-11 mutant hermaphrodites are mated to Hawaiian males to generate F1 progeny that are heterozygous at each SNP. F1 progeny self-replicate to produce recombinant F2 progeny. F2 progeny are then selected for WGS analysis based on the *dec-11* mutant phenotype. Recombination events on the chromosome bearing the phenotype-causing mutation will not occur in close proximity to the *dec-11* mutation, shown as an aqua diamond. Recombination frequency is determined using the CloudMap workflow to isolate the interval containing the *dec-11* mutation. This image is modified from Minevich et al., 2012.

Analysis of the WGS results, using CloudMap, is currently in progress. To date, an error in the server algorithm has prevented us from successfully analyzing our WGS data with the published workflow. This has prevented us from successfully subtracting the Hawaiian SNPs from the whole-genome sequencing results, and identifying a refined candidate gene list.

Alternatively, we have also employed a more conventional approach to WGS analysis. Using the interval determined by SNP interval mapping (Figure 11), we have identified genes with supposed premature stop- and nonsynonymous amino acid mutations (Table 3). However, the Hawaiian DNA incorporated into the experimental DNA through mating may be interfering with the correct identification of mutations, for example if a particular gene is mutated in the Hawaiian background and not the Bristol background. One candidate gene, Y73F8A.23, had a premature stop codon mutation according to WGS, and was analyzed using RNAi and re-sequencing. RNAi analysis of this gene did not phenocopy the *dec-11* mutant phenotype (Figure 12). Additionally, the re-sequencing analysis revealed that Y73F8A.23 was wild-type in *dec-11* homozygous DNA. Presumably, the premature stop codon mutation seen in Y73F8A.23 is a variation specific to the Hawaiian (CB4856) strain. However no confirmed Hawaiian SNP corresponds with the variation in Y73F8A.23 identified by WGS. The candidate genes identified by WGS were cross-referenced to Washington University in St. Louis' Genome Institute database of confirmed Hawaiian SNPs, in order to remove natural Hawaiian variants. However the database contains only confirmed SNPs, therefore some genes present in the revised candidate gene list may still be natural Hawaiian variants.

Table 3. WGS Refined *dec-11* Candidate Gene List

Gene ID	Gene Name	Gene Description	Mutation
Y105C5B.16	*lgc-19*	Ligand-Gated Ion Channel	NonSynonymous Amino Acid Substitution
Y73F8A.25*	*ntl-11*	Ortholog of human CCR4-NOT transcription complex	NonSynonymous Amino Acid Substitution
Y105C5B.13*	*skr-10*	Homolog of SKp1 in *S. cerevisiae*	NonSynonymous Amino Acid Substitution
Y105C5B.6*	*srv-15*	Serpentine Receptor	NonSynonymous Amino Acid Substitution
Y73F8A.16*	*tbx-39*	T BoX family, expressed in intestine	NonSynonymous Amino Acid Substitution
Y73F8A.22*		Predicted protein coding	NonSynonymous Amino Acid Substitution
Y73F8A.26*		Predicted protein coding	NonSynonymous Amino Acid Substitution
Y73F8A.32*		Predicted protein coding	NonSynonymous Amino Acid Substitution
Y73F8A.35		Predicted protein coding	NonSynonymous Amino Acid Substitution
Y105C5A.1*		Predicted protein coding	NonSynonymous Amino Acid Substitution
Y105C5A.8		Predicted protein coding	NonSynonymous Amino Acid Substitution
Y105C5A.9*		Predicted protein coding	NonSynonymous Amino Acid Substitution
Y105C5A.13*		Predicted protein coding	NonSynonymous Amino Acid Substitution
Y105C5A.15		Predicted protein coding	NonSynonymous Amino Acid Substitution
Y105C5A.22		Predicted protein coding	NonSynonymous Amino Acid Substitution
Y105C5A.24		Predicted protein coding	NonSynonymous Amino Acid Substitution
Y105C5B.3		Predicted protein coding	NonSynonymous Amino Acid Substitution
Y105C5B.8*		Predicted protein coding	NonSynonymous Amino Acid Substitution
Y105C5B.11*		Predicted protein coding	NonSynonymous Amino Acid Substitution
Y105C5B.14*		Predicted protein coding	NonSynonymous Amino Acid Substitution
Y105C5B.15*		Predicted protein coding	NonSynonymous Amino Acid Substitution
Y105C5B.19*		Predicted protein coding	NonSynonymous Amino Acid Substitution
Y73F8A.23*		Pseudogene	NonSynonymous Amino Acid Substitution

*Genes analyzed by RNAi

Table 3. WGS Refined *dec-11* Candidate Gene List, *continued*

Y105C5A.2		Pseudogene	NonSynonymous Amino Acid Substitution
Y105C5A.14		Pseudogene	NonSynonymous Amino Acid Substitution
Y105C5A.1282		ncRNA	NonSynonymous Amino Acid Substitution

*Genes analyzed by RNAi

IV. DISCUSSION

In this work, I have sought to identify the gene mutated in *dec-11* worms, using genetic and molecular analysis. While the gene mutated in *dec-11* mutant worms has not yet been identified, it has been determined that DEC-11 maintains proper pacemaker function through regulation of either the initiation or refraction steps of the DMP. In addition, SNP mapping and WGS have successfully identified a set of candidate genes that can now be tested.

Defecation analysis of *dec-11* worms demonstrates that DEC-11 is required for normal DMP pacemaker activity

The long and irregular defecation cycles observed in *dec-11* mutant worms compared to the rhythmic defecation cycles seen in wild-type worms, indicates that *dec-11* is required for proper pacemaker function. It is possible that *dec-11* could play a role in the physiology of the intestine, which in turn maintains pacemaker activity. Future studies examining the spatial and temporal expression pattern of *dec-11* will help to address this question.

Defecation videos demonstrate that once initiated, the DMP proceeds normally. This suggests that Ca^{2+}-waves are proceeding from the posterior intestine in the anterior direction to properly execute all steps of the DMP. Also, Ca^{2+}-waves are only initiated from the pacemaker, and not ectopically, since ectopic Ca^{2+}-waves that fail to initiate a full DMP are known to cause extra, sometimes weak pBoc events (Kemp et al., 2012). However, Ca^{2+} transients must be visualized in order to confirm or refute this conclusion.

Thus, *dec-11* may play a role in regulation of the initiation of Ca^{2+} influx into the pacemaker cell.

Alternatively, *dec-11* may function to regulate the refractory period, in which Ca^{2+} concentration is restored and the system is 'reset' so that the pacemaker can be activated for subsequent defecation cycles. If the refractory period is lengthened in *dec-11* worms, then long and irregular defecation cycles would be expected. As stated previously, CaMKII possibly functions to suppress plasma membrane oscillations, which oscillate faster than the observed DMP period (Nehrke et al., 2008). CaMKII loss-of-function mutations abolish the ability of CaMKII to inhibit plasma membrane oscillations that result in "shadow" pBocs (Nehrke et al., 2008). It is possible that *dec-11* functions to inhibit the activity of CaMKII, so that loss-of-function mutations in *dec-11* could result in overactive CaMKII. Over activity CaMKII could be consistent with the lengthened interval between defecation cycles that is observed in *dec-11* worms.

To distinguish between initiation and refractory defects, electrophysiology and Ca^{2+} imaging in *dec-11* mutant worms could be employed. Electrophysiology could test GON-2/GTL-1 function. If GON-2/GTL-1 currents are unaffected in *dec-11* worms, it may suggest that *dec-11* does not affect initiation of the DMP by regulating either of the TRPM channels. Additionally, if Ca^{2+} imaging reveals a prolonged elevation of intracellular Ca^{2+} in *dec-11* worms, you may conclude that *dec-11* functions to regulate the clearance, and/or refraction of the DMP.

Suppression of the *dec-11* mutant defecation phenotype suggests a role for *dec-11* in the regulation of DMP initiation or refraction

The *dec-11* mutant defecation phenotype could be suppressed by mutations in either of the two IP_3-pathway genes, *ipp-5* or *lfe-2.* The suppression of the *dec-11* mutant phenotype by artificially increasing intracellular levels of IP_3, with *ipp-5* or *lfe-2* loss-of-function mutations, indicates that *dec-11* functions upstream of, or in parallel to, ITR-1-mediated Ca^{2+} release. It is possible that heightened IP_3 levels compensate for defective or absent *dec-11* activity in initiating the DMP, which would reduce the variability of defecation cycles observed in *dec-11* mutants.

The mutant defecation phenotype observed in *dec-11* worms was also suppressed by culturing the mutants on high Mg^{2+} plates. Previously published data, using GON-2 and GTL-1 mutant worms, demonstrated that loss-of-functions mutations in these TRPM channels could be suppressed by supplementation of high Mg^{2+} but not high Ca^{2+}. Additionally, embryonic stem cells from mice lacking functional TRPM7 channels, which are homologous with GON-2, display growth inhibition that can be restored by supplementation of high Mg^{2+} (Paravicini et al., 2012). Mg^{2+} may function to maintain the physiological integrity of cells by regulating ion homeostasis, although the molecular mechanism underlying the role of Mg^{2+} on cellular processes remains unknown.

High extracellular Mg^{2+} suppression of the *dec-11* phenotype, taken together with IP_3 epistasis data, suggests that *dec-11* functions to regulate either initiation or refraction of the DMP. We propose the following models to explain possible regulatory roles of *dec-11* on the DMP. As demonstrated, suppression of the *dec-11* mutant phenotype by supplementation with high Mg^{2+} suggests that *dec-11* may modulate TRPM channel

activity, stability, or localization in the membrane (Figure 14A). Another potential role for *dec-11* is through the regulation of an unidentified membrane component, such as another ion channel or serpentine receptor (Figure 14B), or that *dec-11* encodes an ion channel or serpentine receptor, or an unidentified membrane component (Figure 14C). Finally, the suppression of the mutant defecation cycles observed in *dec-11* worms by artificially increasing IP_3 levels, suggests *dec-11* may function to regulate an intermediary step between Ca^{2+} entry and IP_3 production (Figure 14D).

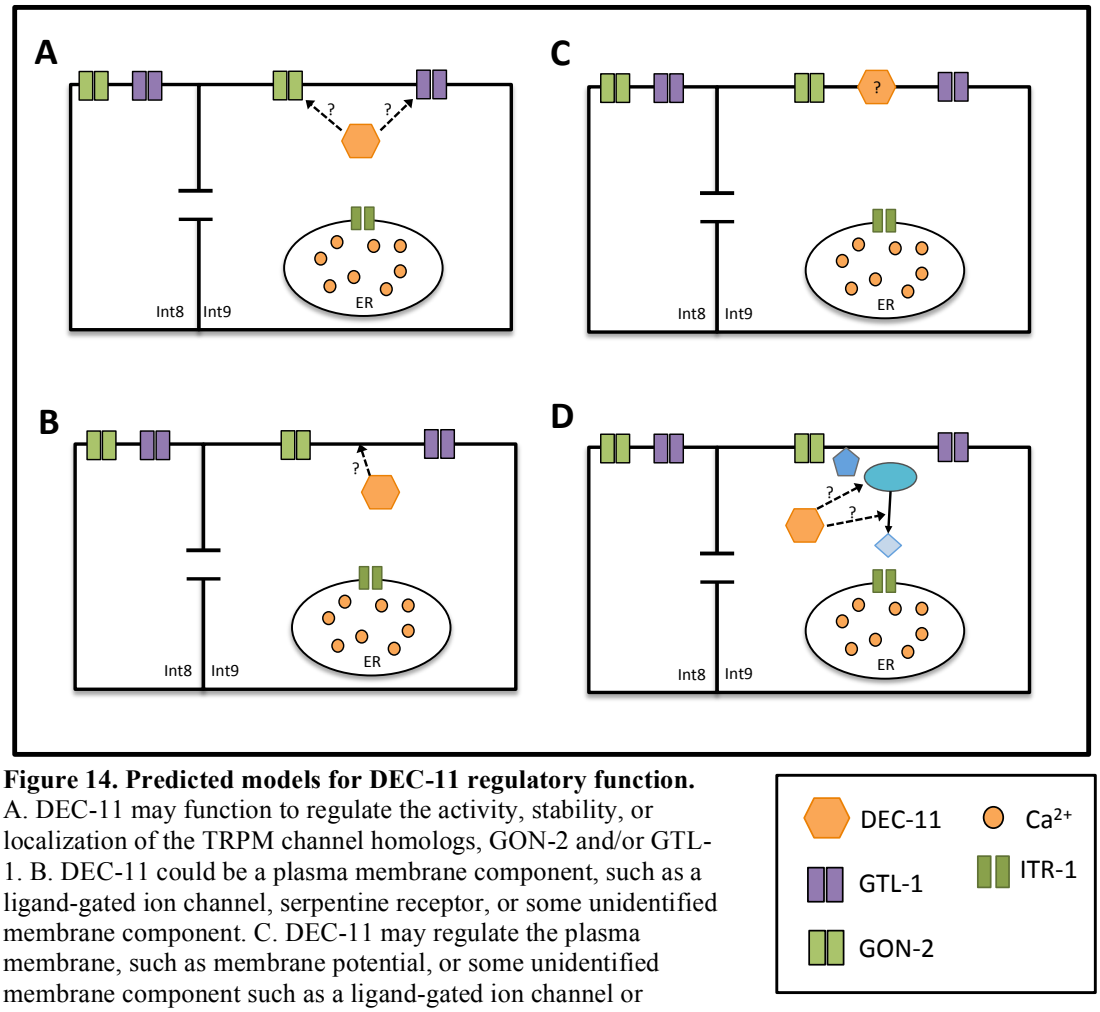

Figure 14. Predicted models for DEC-11 regulatory function. A. DEC-11 may function to regulate the activity, stability, or localization of the TRPM channel homologs, GON-2 and/or GTL-1. B. DEC-11 could be a plasma membrane component, such as a ligand-gated ion channel, serpentine receptor, or some unidentified membrane component. C. DEC-11 may regulate the plasma membrane, such as membrane potential, or some unidentified membrane component such as a ligand-gated ion channel or serpentine receptor. D. DEC-11 may alter the activity of PLCγ to alter IP_3 levels, or some other component of the IP_3 pathway that works upstream or in parallel to ITR-1-mediated Ca^{2+} release.

SNP Interval Mapping tentatively refined the interval containing *dec-11*

By analyzing specific SNPs along the right arm of chromosome IV, for the presence of Hawaiian or Bristol isolate SNPs, we were able to refine the genetic interval in which *dec-11* is located. Based on recombination events, we were able to determine right and left boundaries for the interval containing *dec-11* located at nucleotides 15,321,502 and 16,020,020, respectively. Based on the results of SNP interval mapping we prioritized a set of 62 candidate genes, of which 40 were analyzed using RNAi. All RNAi analysis yielded negative results; no candidate gene analyzed phenocopied the *dec-11* mutant defecation phenotype. Of the 43 worms tested for SNP composition, 9 individuals were identified as recombinant at different SNPS. The simplest explanation for the failure of RNAi to identify the gene mutated in *dec-11* worms is that none of the candidate genes analyzed correspond with *dec-11*. Since RNAi knocks down the expression of candidate genes, this most closely parallels null mutations. If *dec-11* is not a null mutation but is instead a loss-of-function mutation, knockdown with RNAi would not phenocopy the phenotype observed in *dec-11* worms. Alternatively, if *dec-11* is a gain-of-function mutation, RNAi will not phenocopy the *dec-11* mutant phenotype.

Whole-Genome Sequencing identifies candidate genes

Genomic DNA, to be analyzed by WGS, was generated according to the strategy published by Doitsidou et al. (2010), in order to identify the phenotype-causing mutation in a mutagenized strain of *C. elegans*. The WGS results generated by this technique could then be analyzed using the CloudMap workflow (Minevich et al., 2012). However, our attempts to analyze our WGS results with CloudMap have been unsuccessful due to an

error in the server. This has prevented us from subtracting Hawaiian SNPs from the *dec-11* Bristol variant DNA, preventing us from identifying the phenotype-causing mutation in the *dec-11* worms. We are currently investigating alternative methods that will allow us to successfully utilize the CloudMap workflow.

Alternatively, we have been using the bioinformatic analysis provided by the WGS company BGI Americas, to try and identify possibly phenotype-causing mutations such as premature stop codon mutations and nonsynonymous amino acid mutations. However, the bioinformatic data includes gene variants present in the Hawaiian DNA, which makes the data noisy. As seen with the re-sequencing of Y73F8A.23, according to WGS results this gene had a premature stop codon, but when re-sequenced with *dec-11* homozygous DNA there was no mutation. Therefore, it is of utmost importance that we find a successful method of using CloudMap so that we can subtract all Hawaiian background noise from the WGS data to more accurately identify the phenotype-causing mutations in the *dec-11* Bristol DNA.

Future Directions

Future work directed at the identification of *dec-11* will include re-sequencing the candidate mutation in *dec-11* worms to confirm the WGS data, using RNAi analysis of the candidate genes, and rescue experiments to re-introduce a wild-type copy of the candidate gene to suppress defecation defects in *dec-11* mutant worms. Additionally, once the molecular location and identity of *dec-11* has been determined, we will be able to perform expression analysis using a *dec-11*-promoter fusion protein, *dec-11::gfp*. Expression analysis will allow us to determine when and where *dec-11* is expressed, in

order to more fully understand the role of *dec-11* in maintaining pacemaker activity. This work will advance our understanding of pacemaker activity in *C. elegans* and may suggest new pathways that can control ultradian rhythmic behaviors in other organisms.

V. STATEMENT OF METHODOLOGY

C. elegans Culture and Strains

C. elegans strains were maintained at 20°C and 24°C on NGM media plates (1mM $CaCl_2$, 1mM $MgSO_4$, 25mM Potassium Phosphate) cultured with *Escherichia coli* strain AMA1004 under standard conditions (Brenner, 1974). Strains used are listed in Table 4.

Table 4. Strains

Strain Name	Description	Full Genotype
N2	wild-type isolate: Bristol	
JT292	*dec-11* (x2)	*dec-11(sa292) IV*
CB4856	wild isolate: Hawaii	
RF524	*lfe-2 unc-38*	*lfe-2(sy326)unc-38(x20) I*
PS3653	*ipp-5*	*ipp-5(sy605) X*
JK2958	*nT1[qIs51]* IV;V balancer	*nT1[qls51] (IV;V)/ dpy-5(e224) unc-42(e270) V*
RF850	*dec-11; lfe-2*	*dec-11(sa292) IV; lfe-2(sy326) I unc-38(x20) I*
RF853	*dec-11; ipp-5*	*dec-11(sa292) IV; ipp-5(sy605) X*
RF805	*hT2/gon-2; gtl-1*	*hT2/gon-2(g362) I; hT2/+ III; gtl-1(ok375) IV*
RF806	*gon-2; gtl-1*	*gon-2(q362) I; gtl-1(ok375) IV*

Table 5. Primers

Name	Sequence	Category	Notes	Gene/SNP
E6	GACACGACTTTAGAAACAACAGC	SNP Interval Mapping	Forward	F49E11
F6	TGGTATGGAGTCCCTATTTTGG	SNP Interval Mapping	Reverse	F49E12
E7	TGTAAATACCCCACATTTCAAGC	SNP Interval Mapping	Forward	Y57G11B
F7	AAATTTCCAATTGTTCAAAGCC	SNP Interval Mapping	Reverse	Y57G11B
E8	TCGAATTGTTGTGTTTCTTTTGA	SNP Interval Mapping	Forward	Y105C5B
F8	TTCCAATTTTCTCGGTTTGG	SNP Interval Mapping	Reverse	Y105C5B
AA1196	CCGTATCCATCATGTTAAGGTC	SNP Interval Mapping	Forward	Y57G11C
AA1197	AGGAAAATTAGTGGAAGGAAGC	SNP Interval Mapping	Reverse	Y57G11C
AA1198	GCGTTACCCTACTTATGTCCAC	SNP Interval Mapping	Forward	Y41E3
AA1199	AAGTAGCTTCGTAACTGCGC	SNP Interval Mapping	Reverse	Y41E3
AA1200	TTATAACCATTAAGCACGGCC	SNP Interval Mapping	Forward	Y73F8A
AA1201	CCATAAAACAGTCAGCAAATGC	SNP Interval Mapping	Reverse	Y73F8A
AA1202	TGGTCACACACAACAAAGGC	SNP Interval Mapping	Forward	Y105C5A
AA1203	GAAACTCAAAGAAACCGGCG	SNP Interval Mapping	Reverse	Y105C5A
AA782	GCTATTCGTTTGTTTGCGGATAG	*ipp-5* Genotyping	Forward	*ipp-5*
AA783	GAATTGAGAAACGTTCGACCAC	*ipp-5* Genotyping	Reverse	*ipp-5*
AA784	GACTATGAGACATTGCGTGAGTTC	*ipp-5* Genotyping	Reverse-deletion	*ipp-5* deletion
AA1255	TAATACGACTCACTATAGGGAGAAG AAGAGGAAATTGTTTGCGTGAAT	RNAi Constructs	Forward	T7+ *Y73F8A.21*
AA1256	ATTTAAAATGTGTTGCGAGTCTGGT	RNAi Constructs	Reverse	*Y73F8A.21*
AA1257	TAATACGACTCACTATAGGGAGATC ATTTTTCAGATTGCTCAATGGCT	RNAi Constructs	Forward	T7+ *Y73F8A.30*
AA1258	AAGCTGATTATGTGGAAAAAGTGCA	RNAi Constructs	Reverse	*Y73F8A.30*
AA1259	TAATACGACTCACTATAGGGAGATCT TCTTGCTTCTAGCCTTCTTCTT	RNAi Constructs	Forward	T7+ *Y105C5A.3*
AA1260	CATTGGTTGTTGTTGTTGAATGCAT	RNAi Constructs	Reverse	*Y105C5A.3*
AA1261	TAATACGACTCACTATAGGGAGATTC TTCTTGTGGAGGTACGATTTCT	RNAi Constructs	Forward	T7+ *Y105C5A.4*
AA1262	CATTGGTTGTTGTTGTTGAATGCAT	RNAi Constructs	Reverse	*Y105C5A.4*
AA1263	TAATACGACTCACTATAGGGAGATCT TCTTGCTTCTAGCCTTCTTCTT	RNAi Constructs	Forward	T7+ *Y105C5A.6*
AA1264	CATTGGTTGTTGTTGTTGAATGCAT	RNAi Constructs	Reverse	*Y105C5A.6*

Table 5. Primers, *continued*

AA1265	TAATACGACTCACTATAGGGAGAGA CAACAATTTATGCAGCGATTTCC	RNAi Constructs	Forward	T7+ *Y105C5B.2*
AA1266	CAGCAAAAGAACTCGGTTTCAAAAG	RNAi Constructs	Reverse	*Y105C5B.2*
AA1267	TAATACGACTCACTATAGGGAGAAA GTTAAAATCCTGAACGCGTTCTT	RNAi Constructs	Forward	T7+ *Y105C5B.4*
AA1268	GGAATTGTAAACCCAGCAACAGTTA	RNAi Constructs	Reverse	*Y105C5B.4*
AA1269	TAATACGACTCACTATAGGGAGAAC AAACTTTTAGGTATCTGCCAAGC	RNAi Constructs	Forward	T7+ *Y105C5B.10*
AA1270	CGTTGCAGGATATATTTTCGGAGAG	RNAi Constructs	Reverse	*Y105C5B.10*
AA1271	TAATACGACTCACTATAGGGAGAAC GGGTTTCATATGGGATTACGTAT	RNAi Constructs	Forward	T7+ *Y105C5B.16*
AA1272	TGGCATAAATAACTTACCCTCGACA	RNAi Constructs	Reverse	*Y105C5B.16*
AA1332	TAATACGACTCACTATAGGGAGATTG ACAAGAAAAGTGCACGG	RNAi Constructs	Forward	T7+ Y73F8A.23
AA1333	TTTTCCGACAAGGAAAGGAA	RNAi Constructs	Reverse	Y73F8A.23

Strain Construction

The strain with *lfe-2(sy326)* includes the linked *unc-38*(x20) mutation. Thus, *lfe-2(sy326)* was followed using the unc phenotype of *unc-38*(x20) mutant worms while *dec-11(sa292)* was followed using the nT1 balancer from strain JK2958. nT1 is a reciprocal chromosomal translocation on chromosomes IV and V, and includes an integrated GFP transgene. The nT1 balancer precludes homologous recombination of the translocated regions on chromosomes IV and V. This is beneficial, because it allows us to track the presence of *dec-11(sa292)* based on the presence or absence of the GFP signal. A worm heterozygous for nT1[*qls51*] (IV;V)/ *dpy-5(e224) unc-42(e270)* V and *dec-11* will have a GFP signal, but no recombination will occur between the region of chromosome IV containing *dec-11* due to the presence of nT1. Heterozygous worms, when allowed to self-fertilize will then either produce GFP positive progeny or GFP negative progeny. A loss of GFP fluorescence indicates that the animal has lost nT1 and is homozygous for *dec-11*(sa292) on Chromosome IV.

Defecation Scoring

Young adults (within 24 hours of the L4 molt) from both wild-type and mutant strains, were scored at room temperature. The time between each posterior body contraction (pBoc) were scored. The interval between each pBoc is considered 1 cycle, 11 consecutive pBoc events were scored. Statistical analyses were performed using two-tailed t-tests and One-way ANOVA.

Video Microscopy

To examine the events between posterior body contractions, videos were collected using Nikon SMZ-1500 stereomicroscope by capturing images at 10 frames/s for 10 minutes.

SNP Interval Mapping

Interval mapping was performed using the protocol described by Davis et al., 2005. JT292 hermaphrodites were mated to CB4856 males. The F1 progeny from this cross were then bleached to synchronize the F2 progeny. F2-synchronized progeny were picked based on a slow-growth phenotype. F2 mutants were then be cloned to individual plates, allowed to self-replicated, and then the population was lysed, analyzed by PCR with SNP primer pairs (Table 5) and digested with appropriate restriction enzyme, and run on a 2.5% agarose gel.

RNAi by Feeding

RNAi by feeding will be followed according to the protocol described by Ahringer lab (Kamath et al., 2003). The dsDNA for RNAi analysis was generated using plasmid template isolated from either the Ahringer or Vidal RNAi libraries, or Abbott lab construction (Fraser et al., 2000, and Rual et al, 2004). Candidate genes not found in either the Ahringer or Vidal RNAi libraries were constructed using the primers listed in Table 5 and the TA Dual Promoter cloning kit manufactured by Invitrogen. All dsDNA were checked by agarose gel electrophoresis. Young adult N2 F2 progeny were analyzed for defecation defects.

Whole-Genome Sequencing

Whole-genome sequencing was performed according to the "One-step Whole-genome sequencing and SNP mapping strategy" protocol published by Doitsidou et al., 2010. *dec-11* hermaphrodites (JT292), which have a Bristol isolate background, were mated to Hawaiian males (CB4856) to generate heterozygous F1 progeny. F1 progeny were allowed to self-replicate to generate an F2 population. F2 progeny were synchronized to allow for the selection of *dec-11* homozygous mutants, based on their slow-growth phenotype. Selected homozygous mutant F2 progeny were also scored for the *dec-11* mutant defecation phenotype to confirm that they were heterozygous. Selected F2 progeny were cloned and allowed to self-fertilize to generate a pool of recombinant, mutant individuals. The DNA from these pooled individuals was prepped using a Qiagen genomic prep kit and sent for whole-genome-sequencing. Genomic DNA was sent to BGI Tech Solutions Co., Ltd. for whole-genome sequencing. BGI generated a library

using 200 ng DNA inserts. The library was sequenced using Hiseq2000 sequencing protocol to generate paired-end sequencing results. Sequencing results were analyzed by BGI, in reference to a *C. elegans* reference genome using SOAP2.

High Ca^{2+} and Mg^{2+} plates

Wild-type or *dec-11* mutant L4s were transferred to NGM plates containing either 5mM Ca^{2+} or 40mM Mg^{2+}. Young adult F1 progeny were scored for defecation defects, 10 individual worms were scored for 10 defecation cycles. Protocol was performed according to Teramoto et al., 2005.

BIBLIOGRAPHY

Allman, E., Waters, K., Ackroyd, S., and K. Nehrke (2012). Analysis of Ca^{2+} Signaling Motifs That Regulate Proton Signaling through the Na^{+}/H^{+} Exchanger NHX-7 during a Rhythmic Behavior in *Caenorhabditis elegans. Journal of Biological Chemistry,* 288: 8, 5886-5895.

Altun, Z.F. and Hall, D.H. (2009). Alimentary system, intestine. In *WormAtlas*

Beg, A.A., Ernstrom, G.G., Nix, P., Davis, M.W., and E.M. Jorgensen (2008). Protons Act as a Transmitter for Muscle Contraction in *C. elegans*. *Cell,* 132, 149-160.

Branicky, R. and S. Hekimi (2006). What Keeps *C. elegans* regular: the genetics of defecation. *TRENDS in Genetics,* 22:10.

Brenner, S., (1974). The Genetics of *Caenorhabditis elegans. Genetics,* 77, 71-94.

Dal Santo P, Logan M.A., Chisholm A.D., and E.M. Jorgensen (1999). The Inositol Trisphosphate Receptor Regulates a 50-second Behavioral Rhythm in *C. elegans. Cell*, 98, 757-767.

Davis, M.W., Hammarlund, M., Harrach, T., Hullett, P., Olsen, S., and E.M. Jorgensen (2005). Rapid Single Nucleotide polymorphism mapping in *C. elegans*. *BMC Genomics,* 6: 118.

Doitsidou, M., Poole, R.J., Sarin, S., Bigelow, H., and O. Hobert (2010). *C. elegans* Mutant Identification with a One-Step Whole-Genome-Sequencing and SNP Mapping Strategy. *PLoS ONE*, 5:11.

Fleig, A. and R. Penner (2004). The TRPM ion channel subfamily: molecular, biophysical and functional features. *Trends in Pharmacological Sciences,* 25:12, 633-639.

Fraser A.G., Kamath R.S., Zipperlen P., Martinez-Campos M., Sohrmann M., and J. Ahringer (2000). Functional Genomic Analysis of *C. elegans* Chromosome I by Systematic RNAI Interference. *Nature*, 408(6810) 325-30.

Grubbs, R.D., and M.E. Maguire (1987). Magnesium as a Regulatory Cation: Criteria and Evaluation. *Magnesium,* 6, 113-127.

Harteneck, C. (2005). Function and pharmacology of TRPM cation channels. *Naunyn-Schmiedeberg's Arch Pharmacol,* 371, 307-314.

Huizinga, J.D., and W.J.E.P. Lammers (2009). Gut Peristalsis is governed by a multitude of cooperating mechanisms. *American Journal of Physiology-Gastrointestinal and Liver Physiology,* 296, G1-G8.

Iwasaki, K., Liu, D.W.C., and J.H. Thomas (1995). Genes that control a temperature compensated ultradian clock in *Caenorhabditis elegans*. *Proc. Natl. Acad. Sci,* 92, 10317-10321.

Kahn-Kirby, A.H., and C.I. Bargmann (2006). TRP Channels in *C. elegans*. *Annu. Rev. Physiol*, 68, 719-736.

Kamath, R.S. and J. Ahringer (2003). Genome-wide RNAi screening in *Caenorhabditis elegans.* Methods, 30:4, 313-321.

Kemp, B.J., Allman, E., Immerman, L., Mohnen, M., Peters, M.A., Nehrke, K., and A.A. Abbott (2012). miR-786 Regulation of a Fatty-Acid Elongase Contributes to Rhythmic Calcium-Wave Initiation in *C. elegans*. *Current Biology,* 22, 2213-2220.

Komuro, T. (2006). Structure and organization of interstitial cells of Cajal in the gastrointestinal tract. *J Physiol,* 576.3, 653-658.

Kwan, C.S.M., Vásquez-Manrique, R.P., Ly, S., Goyal, K., and H.A. Baylis (2008) TRPM channels are required for rhythmicity in the ultradian defecation rhythm of *C. elegans. BMC Physiology,* 8:11.

McGhee, J.D. The *C. elegans* intestine (March 27, 2007), *WormBook*, ed. The *C. elegans* Research Community, WormBook, doi/10.1895/wormbook.1.133.1, http://www.wormbook.org.

Minevich, G., Park, D.S., Blankenberg, D., Poole, R.J., and O. Hobert (2012). CloudMap: A Cloud-Based Pipeline for Analysis of Mutant Genome Sequences. *Genetics,* 192, 1249-1269.

Nehrke, K., Denton, J., and W. Mowrey (2008). Intestinal Ca^{2+} wave dynamics in freely moving *C. elegans* coordinate execution of a rhythmic motor program. *Am J Physiol,* 294, C333-C344.

Paravicini, T.M., Chubanov, V., and T. Gudermann (2012). TRPM7: A unique channel involved in magnesium homeostasis. *The International Journal of Biochemistry and Cell Biology,* 44, 1381-1384.

Peters, M., Teramoto, T., White, J.Q., Iwasaki, K., and E.M. Jorgensen (2007). A Calcium Wave Mediated by Gap Junctions Coordinates a Rhythmic Behavior in *C. elegans. Current Biology,* 17:18, 1601-1608.

Pfeiffer, J., Johnson, D., and K. Nehrke (2008). Oscillatory Transepithelial H^+ Flux Regulates a Rhythmic Behavior in *C. elegans. Current Biology,* 18, 297-302.

Reiner, D.J., Newton, E.M., Tian, H., and J.H. Thomas (1999). Diverse behavioural defects caused by mutations in *Caenorhabditis elegans unc-43* CaM Kinase II. *Nature*, 402, 199-202.

Rual, J-F., Ceron, J., Koreth, J., Hao, T., Nicot, A-S., Hirozane-Kishikawa, T., Vandenhaute, J., Orkin, S.H., Hill, D.E., van den Heuvel, S., and M. Vidal (2004). Toward Improving *Caenorhabditis elegans* Phenome Mapping With an ORFeome-Based RNAi Library. *Genome Research,* 14:2161-2168/

Rumessen, J.J., Mikkelson, H.B., Qvortrup, K., and L. Thuneberg (1993). Ultrastructure of interstitial cells of Cajal in circular muscle of human small intestine. *Gastroenterology,* 104, 343-350.

Sanders, K.M., Koh, S.D., and S.M. Ward (2006). Interstitial Cells of Cajal as Pacemakers In The Gastrointestinal Tract. *Annu. Rev. Physiol,* 68, 307-343.

Taylor, C.W., and S.C. Tovey (2012). IP_3 Receptors: Toward Understanding Their Activation. *Cold Spring Harb Perspect Biol,* 119-140.

Teramoto, T., Lambie, E.J., and K. Iwaskai (2005). Differential regulation of TRPM channels governs electrolyte homeostasis in the *C. elegans* intestine. *Cell Metabolism,* 1, 343-354.

Teramoto, K., and K. Iwasaki (2006). Intestinal calcium waves coordinate a behavioral motor program in *C. elegans. Cell Calcium,* 40, 319-327.

van der Linden, .M., Beverly, M., Kadener, S., Rodriguez, J., Wasserman, S., Rosbash, M., and P. Sengupta (2010). Genome-Wide Analysis of Light- and Temperature-Entrained Circadian Transcripts in *Caenorhabditis elegans. PLoS,* 8:10.

Wang, H., Girskis, K., Janssen, T., Chan, J.P., Dasgupta, K., Knowles, J.A., Schoofs, L., and D. Sieburth (2013). Neuropeptide Secreted from a Pacemaker Activates Neurons to Control a Rhythmic Behavior. *Current Biology,* 23, 746-754.

Wang, H., and D. Sieburth (2013). PKA Controls Calcium Influx into Motor Neurons during a Rhythmic Behavior. *PLoS Genetics,* 9:9.

Ward, S.M., Ördög, T., Koh, S.D., Abu Baker, S., Jun, J.Y., Amberg, G., Monaghan, K., and K.M. Sanders (2000). Pacemaking in interstitial cells of Cajal depends upon calcium handling by endoplasmic reticulum and mitochondria. *Journal of Physiology,* 525.2, 355-361.

Xing, J., Yan, X., Estevez, A., and K. Strange (2008). Highly Ca^{2+}-selective TRPM Channels Regulated IP_3-dependent Oscillatory Ca^{2+} Signaling in the *C. elegans* Intestine. *J Gen Physiol,* 131: 3, 245-255.

Xing, J., and K. Strange (2010). Phosphatidylinositol 4,5-bisphosphate and loss of PLCγ activity inhibit TRPM channels required for oscillatory Ca^{2+} signaling. *Am J Physiol Cell Physiol,* 298, C2274-C282.

Zhu, M.H., Sung, T.S., O'Driscoll, K., Koh, S.D., and K.M. Sanders (2015). Intracellular Ca^{2+} release from endoplasmic reticulum regulates slow wave currents and pacemaker activity of interstitial cells of Cajal. *Am J Physiol Cell Physiol,* articles in press.